The wiring diagram of a glomerular olfactory system

Matthew E. Berck[1*], Avinash Khandelwal[2*], Lindsey Claus[1], Luis Hernandez-Nuñez[1], Guangwei Si[1], Christopher J. Tabone[1,4], Feng Li[3], James W. Truman[3], Rick D. Fetter[3], Matthieu Louis[2,c], Aravinthan D.T. Samuel[1,c], Albert Cardona[3,c]

January 22, 2016

*: equal contribution.

c: corresponding authors: cardonaa@janelia.hhmi.org, adtsamuel@gmail.com, Matthieu.Louis@crg.eu

1: Harvard University, Department of Physics and Center for Brain Science.

2: EMBL-CRG Systems Biology Program, Centre for Genomic Regulation (CRG), The Barcelona Institute of Science and Technology, Dr. Aiguader 88, 08003 Barcelona, Spain; Universitat Pompeu Fabra (UPF), Barcelona, Spain.

3: HHMI Janelia Research Campus, 19700 Helix Dr., Ashburn, VA 20147.

4: Current address: Fly Base.

Abstract

The sense of smell enables animals to detect and react to long-distance cues according to internalized valences. Odors evoke responses from olfactory receptor neurons (ORNs), whose activities are integrated and processed in olfactory glomeruli and then relayed by projection neurons (PNs) to higher brain centers. The wiring diagram with synaptic resolution, which is unknown for any glomerular olfactory system, would enable the formulation of circuit function hypotheses to explain physiological and behavioral observations. Here, we have mapped with electron microscopy the complete wiring diagram of the left and right antennal lobes of *Drosophila* larva, an olfactory neuropil similar to the vertebrate olfactory bulb. We found two parallel circuits processing ORN inputs. First, a canonical circuit that consists of uniglomerular PNs that relay gain-controlled ORN inputs to the learning and memory center (mushroom body) and the center for innate behaviors (lateral horn). Second, a novel circuit where multiglomerular PNs and hierarchically structured local neurons (LNs) extract complex features from

odor space and relay them to multiple brain areas. We found two types of panglomerular inhibitory LNs: one primarily providing presynaptic inhibition (onto ORNs) and another also providing postsynaptic inhibition (onto PNs), indicating that these two functionally different types of inhibition are susceptible to independent modulation. The wiring diagram revealed an LN circuit that putatively implements a bistable gain control mechanism, which either computes odor saliency through panglomerular inhibition, or allows a subset of glomeruli to respond to faint aversive odors in the presence of strong appetitive odor concentrations. This switch between operational modes is regulated by both neuromodulatory neurons and non-olfactory sensory neurons. Descending neurons from higher brain areas further indicate the context-dependent nature of early olfactory processing. The complete wiring diagram of the first olfactory neuropil of a genetically tractable organism will support detailed experimental and theoretical studies of circuit function towards bridging the gap between circuits and behavior.

Introduction

An animal uses its sense of smell to navigate odor gradients, and to detect the threat or reward associated with an odor. In the nervous system, odors are detected by olfactory receptor neurons (ORNs) whose axons organize centrally into glomeruli by olfactory receptor type (Wang et al., 1998; Vosshall et al., 2000). Uni- and multi-glomerular projection neurons (PNs) relay olfactory inputs to higher-order brain areas (Stocker et al., 1990; Liang et al., 2013). Common between vertebrates and invertebrates (Vosshall and Stocker, 2007; Su et al., 2009), PNs target two major brain centers, one associated with learning and memory (piriform cortex in mammals, mushroom bodies (MB) in insects), and another with innate behaviors (amygdala in mammals, lateral horn (LH) in insects) (Fischbach and Heisenberg, 1984; Heisenberg et al., 1985; Stocker et al., 1990; Sosulski et al., 2011). Local neurons (LNs) mediate communication between glomeruli, implementing computations such as gain control (Olsen and Wilson, 2008). The complete number and morphology of cell types and the circuit structure with synaptic resolution is not known for any glomerular olfactory system.

In the *Drosophila* larva, we find a similarly organized glomerular olfactory system of minimal numerical complexity (fig. 1a). In this tractable system, each glomerulus is defined by a single, uniquely identifiable ORN (Fishilevich et al., 2005; Masuda-Nakagawa et al., 2009) (fig. 1b and supp. fig. 1), and almost all neurons throughout the nervous system are uniquely identifiable and stereotyped (Manning et al., 2012; Vogelstein et al., 2014; H.-H.Li et al., 2014; Ohyama et al., 2015b). Some of the olfactory LNs

and PNs have already been identified (Masuda-Nakagawa et al., 2009; Thum et al., 2011; Das et al., 2013). This minimal glomerular olfactory system exhibits the general capabilities of the more numerically complex systems. For example, as in other organisms (Friedrich and Korsching, 1997; Nagayama et al., 2004; Bhandawat et al., 2007), the output of the uniglomerular PNs tracks the ORN response (Asahina et al., 2009), which represents both the first derivative of the odor concentration and the intensity of the odor (Schulze et al., 2015). Like in the adult fly (Olsen and Wilson, 2008) and zebrafish (Zhu et al., 2013), gain control permits the larval olfactory system to operate over a wide range of odor concentrations (Asahina et al., 2009). The olfactory behaviors exhibited by the larva have been well studied, in particular chemotaxis (Bellmann et al., 2010; Gomez-Marin et al., 2011; Gershow et al., 2012; Schulze et al., 2015; Gepner et al., 2015; Hernandez-Nunez et al., 2015), as have been the odor tuning and physiological responses of ORNs (Fishilevich et al., 2005; Louis et al., 2008; Asahina et al., 2009; Kreher et al., 2008; Montague et al., 2011). Additionally the larva presents odor associative learning (Gerber, 2007). Obtaining the wiring diagram of all neurons synaptically connected to the ORNs would enable the formulation of system-level hypotheses of olfactory circuit function that could explain the observed behavioral and functional properties. The reduced numerical complexity and dimensions of the larval olfactory system, the similarity of its organization and capabilities to other organisms, and the tractability of the larva as a transparent genetic model organism, make it an ideal model system in which to study the complete circuit architecture of a glomerularly organized olfactory processing center.

We reconstructed from electron microscopy all synaptic partners of the 21 ORNs for both the left and right antennal lobes of the larva. Per side, we found 21 uniglomerular PNs (uPNs; one per glomerulus), 14 LNs, 14 multiglomerular PNs (mPNs), 4 neuromodulatory neurons, 6 subesophageal zone (SEZ) interneurons and 1 descending neuron (fig. 1c, d). These identified neurons present stereotyped connectivity when comparing the left and right antennal lobes. Here, we analyze this novel and complete wiring diagram on the basis of the known function of circuit motifs in the adult fly and other organisms and known physiological properties and behavioral roles of identified larval neurons. We found two distinct circuit architectures structured around the two types of PNs: a uniglomerular system where each glomerulus participates in a repeated, canonical circuit, centered on its uPN (Python and Stocker, 2002); and a multiglomerular system where all glomeruli are embedded in structured, heterogeneous circuits read out by mPNs (fig. 1e). We also found that the inhibitory LNs structure a circuit that putatively implements a bistable inhibitory system. One state computes odor saliency through panglomerular lateral inhibition. The other enables select glomeruli, specialized for aversive odors, to

respond to faint stimuli in background of high appetitive odor concentrations. We discuss the role of these two possible operational states and how neuromodulatory neurons and brain feedback neurons modulate the interglomerular circuits.

1 Results

1.1 The uniglomerular system

Olfactory glomeruli are defined by a group of same-receptor ORNs converging onto a set of glomerular-specific PNs (named "mitral cells" in mouse and zebrafish) (Stocker et al., 1990; Satou, 1992; Ressler et al., 1994; Wang et al., 1998; Distler and Boeckh, 1996). In *Drosophila* larva, this system is reduced to a single ORN and a single uPN per glomerulus (Python and Stocker, 2002; Ramaekers et al., 2005; Masuda-Nakagawa et al., 2009). Our EM-reconstructed wiring diagram is in complete agreement with these findings (fig. 1b, 2a). The larval uPNs project to both the center for learning and memory (MB) and the center for innate behaviors (LH; fig. 2a), like in the adult fly and mouse (Stocker et al., 1990; Su et al., 2009; Luo et al., 2010).

1.2 Circuits for interglomerular inhibition

In the adult fly and in vertebrates, the excitation of glomeruli is under control of inhibitory LNs that mediate functions such as gain control, which maintains uPN responses within a dynamic range where odor concentration changes can be detected (Olsen and Wilson, 2008; Olsen et al., 2010; Zhu et al., 2013). We found that most non-sensory inputs to the larval uPNs (fig. 1c) are from a set of 5 panglomerular, axonless, and GABAergic (Thum et al., 2011) neurons that we named Broad LNs (fig. 2b, c; supp. fig. 2). These 5 Broad LNs also account for most inputs onto the ORN axons (fig. 1c), therefore being prime candidates for mediating both intra- and interglomerular presynaptic inhibition (onto ORNs) as observed in the adult fly with morphologically equivalent cells (Wilson and Laurent, 2005; Olsen and Wilson, 2008; Olsen et al., 2010; Chou et al., 2010), and in larva (Asahina et al., 2009).

We divided the 5 Broad LNs into two classes, the Trio and Duet, based on the number of neurons of each type (fig. 2b). While both types provide panglomerular presynaptic inhibition (onto ORN axons), the duet plays a far stronger role in postsynaptic inhibition (onto uPN dendrites; fig. 2d). In

the adult fly, presynaptic inhibition implements gain control (Olsen and Wilson, 2008), and postsynaptic inhibition plays a role in uPNs responding to the change in ORN activity (Nagel et al., 2015; Kim et al., 2015). The two types of glomerular inhibition are provided by two separate cell types, and may therefore be modulated independently. For example, the uPNs emit dendritic outputs that primarily target the Broad LN Trio (fig. 2d), indicating that the output of the glomerulus contributes more to presynaptic than to postsynaptic inhibition. Similar excitatory synapses from uPNs to inhibitory LNs have been shown in vertebrates (Rall et al., 1966).

Beyond their role in pre- and postsynaptic inhibition of ORNs and uPNs respectively, the Broad LNs synapse onto all neurons of the system, including other LNs and mPNs (fig. 1c; supp. fig. 3). Therefore Broad LNs may keep the entire olfactory system within the dynamic range to remain responsive to changes in odor intensities. Importantly, Broad LNs also synapse onto each other (fig. 2c, e) like in the adult (Okada et al., 2009), suggestive of a mechanism for sequential recruitment as overall stimulus intensity increases to maintain uPN output within the dynamic range. Furthermore the two types of Broad LNs have a different ratio of excitation and inhibition, originating in the preference of trio to synapse far more strongly onto each other than onto duet (fig. 2e, supp. fig. 3). This suggests that the two types not only have different circuit roles but also have different properties.

Another GABAergic cell type, the Choosy LNs (two neurons; fig. 1c, 2c, supp. fig. 4; see fig. 2L-O in Thum et al., 2011), contributes exclusively to postsynaptic inhibition for most glomeruli. Unlike the Broad LNs, Choosy LNs are driven by only a small subset of glomeruli (fig. 2c) and have defined axons (supp. fig. 4). Therefore some glomeruli can drive postsynaptic inhibition of most other glomeruli. Additionally, the inputs from Choosy LNs tend to be more proximal to the axon initial segment of the uPNs (Gouwens and Wilson, 2009) unlike those of Broad LNs which are more uniformly distributed throughout the uPN dendritic arbor (supp. fig. 5). This pattern of spatially structured inputs suggests that different inhibitory LN types may exert different effects on uPN dendritic integration.

1.3 Extracting features from odor space at the first synapse

Parallel to the uniglomerular readout by the 21 uPNs, we found 14 multiglomerular PNs (mPNs; fig. 3a). Each mPN receives unique and stereotyped inputs from multiple ORNs (fig. 3c) or at least from one ORN and multiple unidentified non-ORN sensory neurons in the SEZ (fig. 3a). The mPNs originate in multiple neuronal lineages and project to multiple brain regions; most commonly the lateral horn

(LH) but also regions surrounding the MB calyx. Of the 14, three project to the calyx (mPNs b-upper, b-lower and C2) and another (mPN cobra) to the MB vertical lobe (fig. 3a). In addition to the 14 mPNs that project to the brain, we identified an extra 6 oligoglomerular neurons that project to the SEZ (SEZ neurons; fig. 1c; supp. fig. 6). A class of mPNs has been described in the adult fly (Liang et al., 2013) but their projection pattern does not match any of the larval mPNs. In strong contrast to uPNs, mPNs are very diverse in their lineage of origin, their pattern of inputs, and the brain areas they target. A small subset of mPNs has been identified in light microscopy before (Thum et al., 2011; Das et al., 2013).

In addition to inputs from Broad LNs (supp. fig. 2), mPNs also receive up to 26% of inputs from 5 stereotypically connected, oligoglomerular Picky LNs (fig. 3b, c). At least 4 of these 5 Picky LNs are glutamatergic (supp. fig. 7), and they all derive from the same lineage (fig. 3b). Glutamate has been shown to act as a postsynaptic inhibitory neurotransmitter in the adult fly antennal lobe for both PNs and LNs (Liu and Wilson, 2013), and therefore in larva Picky LNs may provide inhibition onto both mPNs and other LNs. Unlike the Broad LNs, which are panglomerular and axonless, the Picky LNs present separated dendrites and axons (fig. 3b). Collectively, Picky LN dendrites roughly tile the antennal lobe (fig. 3b). While some Picky LN axons target select uPNs, about 40% of Picky LN outputs are dedicated to mPNs or each other (fig. 3c; supp. fig. 3). Similarly to the mPNs, Picky LNs 2, 3, and 4 receive inputs from unidentified non-ORN sensory neurons in the SEZ (supp. fig. 3).

Given that ORNs present overlapping odor tuning profiles (Kreher et al., 2008), we applied dimensionality-reduction techniques and discovered that ORNs cluster into 5 groups by odor preference (supp. fig. 8). This helped interpret the pattern of ORNs onto Picky LNs and mPNs. We found that some Picky LNs aggregate similarly responding ORNs (fig. 3d; supp. fig. 9). For example, Picky LN 2 receives inputs preferentially from ORNs that respond to aromatic compounds, and Picky LN 3 and 4 similarly for aliphatic compounds (esters and alcohols; supp. fig. 9). On the other hand, Picky LN 0 and 1 aggregate inputs from ORNs from different clusters, suggesting that these Picky LNs may select for ORNs that are similar in a dimension other than odor preference.

The stereotyped and unique convergence of different sets of ORNs onto both mPNs and Picky LNs, and the selective connections from Picky LNs to mPNs, suggest that each mPN responds to a specific feature in odor space. These features are implemented through direct excitatory connections from ORNs or indirect via Picky LNs (lateral inhibition; fig. 3d). Some ORNs engage in both direct excitatory and lateral inhibitory connections through Picky LNs (incoherent feedforward loop, Alon, 2007; fig. 3d)

to the same mPN. The combination of these motifs may enable an mPN to respond more narrowly to odor stimuli than the ORNs themselves, many of which are broadly tuned (Kreher et al., 2008), or to respond to a combinatorial function of multiple ORNs that describe an evolutionarily learned feature meaningful for the larva.

For example, one mPN (A1) reads out the total output of the uniglomerular system by integrating inputs across most ORNs and uPNs (fig. 3c). Another mPN (B2) could respond to the linear combination of ORNs sensitive to aromatic compounds (direct connections), but its response could change in the presence of alcohols and esters due to feedforward loops (fig. 3d). And mPNs A3 and B3 both collect inputs from ORNs (fig. 3c, d) known to respond to aversive compounds (22c, 45b, 49a, 59a, and 82a; Kreher et al., 2008; Ebrahim et al., 2015) or whose ORN drives negative chemotaxis (45a; Bellmann et al., 2010; Hernandez-Nunez et al., 2015). Additionally, mPN B3 receives inputs from 33a, an ORN whose receptor lacks a known binding compound and therefore is likely narrowly tuned to another ecologically relevant odor like was shown for 49a and the parasitoid odor (Ebrahim et al., 2015). The 14 types of mPNs are vastly diverse from each other and likely each one extracts a very different feature from odor space, often integrating as well inputs from non-ORN sensory neurons.

In contrast to the all-to-all connectivity of the Broad LNs, the Picky LNs synapse onto each other in a selective, hierarchical fashion (fig. 3e). The structure of the Picky LN hierarchy suggests that Picky LNs 0 and 3 can operate in parallel, while the activity of the other Picky LNs is dependent on Picky LN 0 (fig 3e). These connections among Picky LNs include axo-axonic connections, and some Picky LNs receive stereotypic ORN inputs onto their axons (supp. fig. 9). The stereotyped hierarchy among Picky LNs defines yet another layer of computations in the integration function of each mPN.

1.4 Non-ORN sensory neurons and interactions among LNs can alter the operational state of the olfactory system

Picky LN 0 not only dominates the Picky LNs, and with it the multiglomerular system, but also may dramatically alter the inhibition of the entire olfactory system. This is because the main synaptic target of Picky LN 0 (supp. fig. 3) is a bilateral, axonless, GABAergic LN called Keystone (fig. 4a; supp. fig. 7), which in turn strongly synapses onto the Broad LN trio–a major provider of presynaptic inhibition (fig. 4b). Interestingly, Keystone is also a major provider of presynaptic inhibition, but selectively avoids some glomeruli (fig. 4c; supp. fig. 2). Therefore there are two parallel systems for providing presynaptic

inhibition that directly and strongly inhibit each other (fig. 4b): homogeneous across all glomeruli when provided by the Broad LN trio, and heterogeneous when provided by Keystone (fig. 4c). In conclusion, the circuit structure indicates that Picky LN 0 may promote a state of homogeneous presynaptic inhibition by disinhibiting the Broad LN trio (fig. 4d).

The alternative state of heterogeneous presynaptic inhibition implemented by Keystone could be triggered by select non-ORN sensory neurons that synapse onto Keystone in the SEZ (fig. 4a, b). These non-ORN sensory neurons are the top inputs of Keystone and do not synapse onto any other olfactory LN. In contrast, ORNs that synapse onto Keystone also synapse onto the Broad LN trio (supp. fig. 2), suggesting a role for non-ORN sensory inputs in tilting the balance towards Keystone and therefore the heterogeneous state. However, the subset of ORNs that also synapse onto Picky LN 0 (fig. 4e) could oppose the effect of the non-ORN sensory neurons by inhibiting keystone and therefore disinhibiting the Broad LN trio.

Neuromodulatory neurons can also affect the balance between Keystone and Broad LN trio. Beyond the possible effect of volume release of serotonin (Dacks et al., 2009) and octopamine (Linster and Smith, 1997; Selcho et al., 2012) within the olfactory system, we found that these neuromodulatory neurons synapse directly and specifically onto Keystone or Broad LN trio, respectively (fig 4b). Beyond non-ORN inputs, ORNs synapse selectively onto these neuromodulatory neurons. Two ORNs (74a and 82a) synapse onto the serotonergic neuron CSD (Roy et al., 2007), and five ORNs (42b, 74a, 42a, 35a and 1a) onto an octopaminergic neuron (lAL-1; see fig. 4k in (Selcho et al., 2014)), suggesting that specific ORNs may contribute to tilting the balance between homogeneous and heterogeneous presynaptic inhibition via neuromodulation.

The only other provider of panglomerular presynaptic inhibition is the Broad duet, which is the main provider of panglomerular postsynaptic inhibition. These neurons may operate similarly in both states given that they are inhibited by both Keystone and Broad LN trio (fig. 1c). The higher fraction of inputs from Broad LN trio onto duet might be compensated by the fact that the trio LNs inhibit each other (fig. 2e, 4b), whereas the two Keystone LNs do not (fig. 4b). Therefore, potentially the Broad LN duet are similarly active in either state (fig. 4d).

1.5 Some glomeruli are special-purpose

The possibility of heterogeneous presynaptic inhibition promoted by Keystone suggests that some ORNs can escape divisive normalization of their outputs relative to the rest. Not surprisingly, one such ORN is 49a (fig. 4c), which is extremely specific for the sexual pheromone of a parasitic wasp that predates upon larvae (Ebrahim et al., 2015). The other two ORNs that escape fully are 1a and 45b. 1a activation drives negative chemotaxis (Hernandez-Nuñez et al., unpublished). 45b senses compounds that elicit negative chemotaxis in larvae (Kreher et al., 2008). These three ORNs, and in particular 49a, are under strong postsynaptic inhibition by both Broad LN duet and Choosy LNs (fig. 2c). In summary, reducing presynaptic inhibition in these 3 ORNs may enable the larvae to perceive odors evolutionarily associated with life-threatening situations less dependently of the response intensity of other ORNs (i.e. overall odor concentration). This is consistent with the finding that responses to aversive odors may rely on specific activity patterns in individual ORNs (Gao et al., 2015). The strong postsynaptic inhibition might be instrumental for their corresponding uPN to respond to the derivative of the ORN activity (with an incoherent feedforward loop; Alon, 2007), as shown in the adult fly (Kim et al., 2015), facilitating detection of concentration changes.

A key neuron in tilting the balance between homogeneous and heterogeneous presynaptic inhibition is Picky LN 0 (fig. 4b). Remarkably, one of the two top ORN partners of Picky LN 0 is ORN 42a (fig. 2c), the strongest driver of appetitive chemotaxis in larvae (Fishilevich et al., 2005; Asahina et al., 2009; Schulze et al., 2015; Hernandez-Nunez et al., 2015). The connections of Picky LN 0 extend beyond that of other oligoglomerular LNs, and include both pre- and postsynaptic inhibition of a small subset of glomeruli, including 42a (fig. 4e). The wiring diagram therefore indicates that Picky LN 0, a likely glutamatergic LN, engages in seemingly contradictory circuit motifs: simultaneously inhibiting specific ORNs and their uPNs, while also disinhibiting them by inhibiting Keystone. The suppression of Keystone disinhibits the Broad LN Trio and therefore promotes homogeneous inhibition. However this is further nuanced by reciprocal connections between Picky 0 LN and Broad LN Trio (fig. 4b). This push-pull effect of glutamatergic LNs on PNs has been described for the olfactory system of the adult fly as conducive to more robust gain control and rapid transitions between network states (Liu and Wilson, 2013). This refined control could endow Picky 0 LN-innervated glomeruli like 42a (fig. 4e) with the ability to better detect odor gradients, consistent with 42a being a strong and reliable driver of appetitive chemotaxis (Fishilevich et al., 2005; Asahina et al., 2009; Schulze et al., 2015).

Picky LN 0 and its push-pull effect on PNs not only can have an effect on positive chemotaxis but also on negative. A clear example is the 82a glomerulus (known to respond to an aversive odor that drives negative chemotaxis (Kreher et al., 2008)) which lacks a well-developed uPN but engages in strong connections with mPNs such as A3 (which aggregates aversive inputs, see above; fig. 3c). We found that, like for the appetitive case of 42a, Picky LN 0 engages in both presynaptic inhibition onto 82a ORN and also postsynaptic inhibition onto mPN A3, one of the top PNs of 82a ORN. And like other ORNs mediating aversive responses (e.g 49a), the 82a uPN is also under strong postsynaptic inhibition (fig 2c).

Finally, an individual glomerulus can have a global effect on the olfactory system. All LNs receive inputs from Ventral LN (fig. 1c, supp. fig. 4), an interneuron of unknown neurotransmitter, which is primarily driven by the 13a glomerulus. This suggest that 13a, an ORN sensitive to alcohols (Kreher et al., 2008), could potentially alter the overall olfactory processing.

1.6 Feedback from the brain

In the mammalian olfactory bulb, descending inputs from the brain target granule cells (the multiglomerular inhibitory LNs), shaping the level of inhibition (Balu et al., 2007). In addition to descending neuromodulatory neurons (CSD; fig. 4a), in the larva we found a descending neuron (supp. fig. 4) that targets specific mPNs and LNs (supp. fig. 2). In addition to other mPNs, this descending neuron targets the two mPNs that we postulate are aversive (mPNs A3 and B3). Together with the axo-axonic inputs it receives from 45a ORN (an aversive ORN, (Bellmann et al., 2010; Hernandez-Nunez et al., 2015)), this descending neuron is clearly associated with the processing of aversive stimuli. Additional descending neurons affecting PNs and LNs might exist but were beyond the scope of this study, where we focused on neurons directly synapsing with ORNs.

Discussion

The glomerular olfactory system of the larva develops in a similar fashion to the vertebrate olfactory bulb where the afferents (i.e. ORNs) organize the central neurons, unlike in the adult fly (Prieto-Godino et al., 2012). In zebrafish, GABAergic LNs provide depolarizing currents to PNs (mitral cells) via gap junctions at low stimulus intensities, enhancing low signals, and inhibit the same PNs at high stimulus

intensity via GABA release, implementing a form of gain control (Zhu et al., 2013). This role is played by a panglomerular excitatory LN in the adult fly that makes gap junctions onto PNs and excites inhibitory LNs (Yaksi and Wilson, 2010). In the larva, all panglomerular neurons are GABAergic; if any were to present gap junctions with uPNs, a cell type for gain control in larva would be equivalent to the one in zebrafish. Particularly good candidates are the Broad LN duet, which provide the bulk of feedforward inhibitory synapses onto uPNs in larva. Interestingly, postsynaptic inhibition might not be mediated by GABA in the adult fly (supp. fig. 5 in Olsen and Wilson, 2008), rendering olfactory circuits in larva more similar to vertebrates. Presynaptic inhibition exists both in the adult fly and, as we have shown, in larva, and is mediated by the same kind of panglomerular GABAergic neurons (the trio LNs in larva; and see (Olsen and Wilson, 2008)).

The uniglomerular circuit is the most studied in all species both anatomically and physiologically. We found that each uPN receives an unusually large number of inputs from an individual ORN compared to other sensory systems in the larva (Ohyama et al., 2015a). This large number of morphological synapses could be interpreted as a strong connection, which would support faster or more reliable signal transmission. In the adult fly, the convergence of multiple ORNs onto an individual PN enables both a fast and reliable PN response to odors (Bhandawat et al., 2007)). The temporal dynamics of crawling are far slower than that of flying, and therefore we speculate that the integration over time of the output of a single ORN might suffice for reliability, demanding only numerous synapses to avoid saturation.

Positive, appetitive chemotaxis involves odor gradient navigation, leading to a goal area where food is abundant which may overwhelm olfaction. We postulate that navigation and feeding correspond to the homogeneous and heterogeneous states of presynaptic inhibition that we described. During navigation, homogeneous presynaptic inhibition (via Broad LN trio) could best enhance salient stimuli and therefore chemotaxis, enabling the olfactory system to operate over a wide range of odor intensities (Asahina et al., 2009). During feeding, strongly stimulated ORNs could scale down the inputs provided by other, less stimulated, ORNs. In other words, if homogeneous presynaptic inhibition persisted during feeding, the larvae would lose the ability to detect important odors that are likely to be faint, for example the scent of a predator such as a parasitic wasp via 49a (Ebrahim et al., 2015). The larvae can selectively release presynaptic inhibition via Keystone, which provides presynaptic inhibition to appetitive glomeruli while also inhibiting the Broad LN trio–the major providers of panglomerular presynaptic inhibition. So the larva could feed and remain vigilant to evolutionarily important cues at

the same time. Not surprisingly, the switch might be triggered by the neuromodulatory neurons and non-ORN sensory neurons, potentially gustatory, that synapse onto Keystone.

In addition to the uniglomerular system that is present across multiple vertebrate and invertebrate species (Satou, 1992; Wang et al., 1998; Vosshall et al., 2000), we found, in the *Drosophila* larva, a multiglomerular system that presumably performs diverse processing tasks already at the first synapse. One such task could be the detection of concentration gradients for some odor mixtures, suggesting an explanation for the observation that some ORNs can only drive chemotaxis when co-activated with other ORNs (Fishilevich et al., 2005). Similar glomerular-mixing circuits have been described in higher brain areas (lateral horn) of the fly (Wong et al., 2002; Fişek and Wilson, 2014) and of mammals (Sosulski et al., 2011). We hypothesize that in the larva, the morphological adaptations to a life of burrowing might have led to specific adaptations, relevant to an animal that eats with its head, and therefore the dorsal organ housing the ORNs, embedded in food. It is perhaps not surprising that we found multisensory integration across ORNs and non-ORNs (likely gustatory) already at the first synapse. And we hypothesize that the pooling of chemosensors (ORNs and non-ORNs) onto mPNs and Picky LNs may be related to the reduction in the number of ORNs relative to insects with airborne antennae.

With our complete wiring diagram of this tractable, transparent model system and genetic tools for manipulating and monitoring the activity of single identified neurons, we have now the opportunity to bridge the gap between neural circuits and behavior (Carandini, 2012).

2 Materials and methods

2.1 Electron microscopy and circuit reconstruction

We reconstructed neurons and annotated synapses in a single, complete central nervous system from a 6-h-old $[iso]$ *Canton S G1 x* w^{1118} larva imaged at 4.4 x 4.4 x 50 nm resolution, as described in Ohyama et al., 2015a. The volume is available at http://openconnecto.me/catmaid/, titled "acardona_0111_8". To map the wiring diagram we used the web-based software CATMAID (Saalfeld et al., 2009), updated with the novel suite of neuron skeletonization and analysis tools (Schneider-Mizell et al., 2015), and applied the iterative reconstruction method described in Ohyama et al., 2015a; Schneider-Mizell et al., 2015. In all, we reconstructed 128 neuronal arbors for a total of 37,284 postsynaptic sites and 51.7 milimiters of cable, requiring about 600,000 mouse clicks over 705 hours of reconstruction and 409 hours of review. Only

375 (1%) of postsynaptic sites remained on small arbor fragments (0.3 milimiters of cable, or 0.5%) that could not be assigned to any neuron.

2.2 Immunolabeling and light microscopy

CNS was dissected from 3rd instar larvae. 4% formaldehyde was used as fixative for all anitbodies except anti-dVGlut that required bouin fixation (Drobysheva et al., 2008). After fixation, brain samples were stained with rat anti-flag (1:600, Novus Biologics) and chicken anti-HA (1:500, Abcam, ab9111) for labeling individual neurons in the multi-color flip-out system (Nern et al., 2015), while mouse anti-Chat (1:150, Developmental Studies Hybridoma Bank, ChaT4B1) and rabbit anti-GABA (1:500, Sigma A2052, Lot# 103M4793) or anti-dVGlut (Daniels et al., 2004) were used for identifying neurotransmitters. Antibodies were incubated at 4oC for 24 hours. Preparations were then washed 3 times for 30 min. with 1% PBT and then incubated with secondary antibodies (including: goat anti-Mouse Alexa Fluor 488, goat anti-rabbit Alexa Fluor 568, donkey anti-rat Alexa Fluor 647, Thermfisher; and goat anti-chicken Alexa Fluor 405, Abcam) at 1/500 for 2 hours at room temperature, followed by further washes. Nervous systems were mounted in Vectashield (Vector Labs) and imaged with a laser-scanning confocal microscope (Zeiss LSM 710).

2.3 Clustering of ORNs by PCA of their responses to odors

Odors are spatiotemporally encoded in neural activity patterns of olfactory receptor neurons. It has been shown, however, that odor information is also encoded in the global response of the ORN population (without taking timing into account) (Haddad et al., 2010). Since the *Drosophila* larva only has 21 ORNs and there have been extensive studies that show the responses of these neurons to many odors (Kreher et al., 2008; Montague et al., 2011; Mathew et al., 2013), we reanalyzed this data using dimensionality reduction techniques (PCA) and clustering algorithms to establish how the 21 ORNs encode odor chemical descriptor space.

Our strategy was to conduct the analysis with the data from Kreher et al., 2008 and Montague et al., 2011 and use the data in Mathew et al., 2013 to verify our conclusions. First, we identified the location of as many odors as we could (Kreher et al., 2008; Montague et al., 2011) in the 32 dimensional chemical descriptor space proposed in Haddad et al., 2008. We looked up the descriptors for the odors

used in the database provided in Haddad et al., 2008 and found descriptors for 32 odors. To find out how these odors segregate in the 32 dimensional space we conducted K-means clustering. We found that clustering is well correlated with the chemical type of the odor: one cluster has mainly esters, another one alcohols, 2 clusters have mainly aromatics and another one pyrazines (supp. fig. 8a).

We next addressed how ORNs encode odor space. For instance, whether each ORN encodes a different region of odor space; whether different groups of ORNs encode different regions of odor space; whether only a few ORNs encode different regions and other ones encode everything. First, we followed the PCA analysis proposed in (Haddad et al., 2010) (where only total firing rate is considered but not timing). Since the data from Kreher et al., 2008 and Montague et al., 2011 was collected using the empty neuron system, for ORNs that express 2 odor receptors (in addition to ORCO), such as OR47a/OR33b, we considered the maximum observed firing rate. Then we asked how global odor representation in the 21 ORN space was segregated. We reduced the dimension of the space and kept the meaningful dimensions. We selected 3 principal components based on the Scree Test (only use the principal components that form the elbow of supp. fig. 8b). Afterwards, we used the affinity propagation clustering algorithm (which doesn't specify a number of clusters as an input) and found that it converged to 5 clusters (supp. fig. 8c).

The clusters in odor space also correlate very well with the chemical type (supp. fig. 8d). Importantly, the clusters in ORN-PCA feature space also correspond very well with the ones found in chemical descriptor space proposed in Haddad et al., 2008, suggesting that different sets of ORNs encode each of the 5 regions of the odors in chemical descriptor space. In order to identify which ORNs encode each region, we represented each cluster with its centroid and projected this point back to ORN space. We found that the centroid of each cluster is represented by subsets of ORNs (supp. fig. 8d). The projection of the cluster centroids in ORN space is not a discrete number; in order to make this results easier to interpret a threshold can be established to determine which ORNs encode a cluster centroid and which ones don't. One way of doing this is by using Otsu's method, which can be considered a one-dimensional discrete analog of Fisher's discriminant analysis (Otsu, 1975). We obtained a threshold of 0.4725, which we used to determine the ORNs that encode each cluster (supp. fig. 8e).

Acknowledgements

We thank Ingrid Andrade, Anton Miroschnikow, Ilona Brueckmann, Ivan Larderet, Volker Hartenstein, Bruno Afonso and Philipp Schlegel for contributing 15.5% of all reconstructed arbor cable, and Gaetan Vignoud for assistance with the PCA. We thank Rachel Wilson, Kathy Nagel, Andreas Thum, Bertram Gerber, Markus Knaden and Ibrahim Tastekin for constructive comments and discussions. A.D.T.S. thanks "The Harvard Brain Initiative Collaborative Seed Grant Program", the NIH Pioneer Award (8DP1GM105383), NIH PO1 (1P01GM103770), NSF BRAIN Initiative (NSF- IOS-1556388) and Harvard Brain Initiative Collaborative Seed Grant. M.E.B thanks the NSF Physics of Living Systems Student Network. M.L. and A.K. acknowledge support of the Spanish Ministry of Economy and Competitiveness, 'Centro de Excelencia Severo Ochoa 2013-2017', SEV-2012-0208 and grants MICINN BFU2011-26208. AK acknowledges the support of the 'laCaixa' International PhD programme. We thank the Fly EM Project Team at HHMI Janelia for the gift of the EM volume, the HHMI visa office, and HHMI Janelia for funding.

References

Alon, U. (2007). Network motif: theory and experimental approaches. *Nature Reviews Genetics*, 8(6):450–61.

Asahina, K., Louis, M., Piccinotti, S., and Vosshall, L. B. (2009). A circuit supporting concentration-invariant odor perception in drosophila. *Journal of biology*, 8(1):9.

Balu, R., Pressler, R. T., and Strowbridge, B. W. (2007). Multiple modes of synaptic excitation of olfactory bulb granule cells. *The Journal of neuroscience*, 27(21):5621–5632.

Bellmann, D., Richardt, A., Freyberger, R., Nuwal, N., Schwärzel, M., Fiala, A., and Störtkuhl, K. F. (2010). Optogenetically induced olfactory stimulation in *Drosophila* larvae reveals the neuronal basis of odor-aversion behavior. *Frontiers in behavioral neuroscience*, 4.

Bhandawat, V., Olsen, S. R., Gouwens, N. W., Schlief, M. L., and Wilson, R. I. (2007). Sensory processing in the *Drosophila* antennal lobe increases reliability and separability of ensemble odor representations. *Nature neuroscience*, 10(11):1474–1482.

Carandini, M. (2012). From circuits to behavior: a bridge too far? *Nature neuroscience*, 15(4):507–509.

Chou, Y.-H., Spletter, M. L., Yaksi, E., Leong, J. C., Wilson, R. I., and Luo, L. (2010). Diversity and wiring variability of olfactory local interneurons in the *Drosophila* antennal lobe. *Nature neuroscience*, 13(4):439–449.

Dacks, A. M., Green, D. S., Root, C. M., Nighorn, A. J., and Wang, J. W. (2009). Serotonin modulates olfactory processing in the antennal lobe of drosophila. *Journal of neurogenetics*, 23(4):366–377.

Daniels, R. W., Collins, C. A., Gelfand, M. V., Dant, J., Brooks, E. S., Krantz, D. E., and DiAntonio, A. (2004). Increased expression of the *Drosophila* vesicular glutamate transporter leads to excess glutamate release and a compensatory decrease in quantal content. *The Journal of neuroscience*, 24(46):10466–10474.

Das, A., Gupta, T., Davla, S., Prieto-Godino, L. L., Diegelmann, S., Reddy, O. V., Raghavan, K. V., Reichert, H., Lovick, J., and Hartenstein, V. (2013). Neuroblast lineage-specific origin of the neurons of the *Drosophila* larval olfactory system. *Developmental biology*, 373(2):322–337.

Distler, P. G. and Boeckh, J. (1996). Synaptic connection between olfactory receptor cells and uniglomerular projection neurons in the antennal lobe of the american cockroach, periplaneta americana. *Journal of Comparative Neurology*, 370(1):35–46.

Drobysheva, D., Ameel, K., Welch, B., Ellison, E., Chaichana, K., Hoang, B., Sharma, S., Neckameyer, W., Srinakevitch, I., Murphy, K. J., et al. (2008). An optimized method for histological detection of dopaminergic neurons in *Drosophila* melanogaster. *Journal of Histochemistry & Cytochemistry*, 56(12):1049–1063.

Ebrahim, S., Dweck, H., Stökl, J., Hofferberth, J., Trona, F., Weniger, K., Rybak, J., Seki, Y., Stensmyr, M., Sachse, S., et al. (2015). *Drosophila* avoids parasitoids by sensing their semiochemicals via a dedicated olfactory circuit. *PLoS biology*, 13(12):e1002318.

Fischbach, K. and Heisenberg, M. (1984). Neurogenetics and behaviour in insects. *Journal of experimental biology*, 112(1):65–93.

Fişek, M. and Wilson, R. I. (2014). Stereotyped connectivity and computations in higher-order olfactory neurons. *Nature neuroscience*, 17(2):280–288.

Fishilevich, E., Domingos, A. I., Asahina, K., Naef, F., Vosshall, L. B., and Louis, M. (2005). Chemotaxis behavior mediated by single larval olfactory neurons in drosophila. *Current Biology*, 15(23):2086–2096.

Friedrich, R. W. and Korsching, S. I. (1997). Combinatorial and chemotopic odorant coding in the zebrafish olfactory bulb visualized by optical imaging. *Neuron*, 18(5):737–752.

Gao, X. J., Clandinin, T. R., and Luo, L. (2015). Extremely sparse olfactory inputs are sufficient to mediate innate aversion in *Drosophila*. *PLoS ONE*, 10(4):e0125986.

Gepner, R., Skanata, M. M., Bernat, N. M., Kaplow, M., and Gershow, M. (2015). Computations underlying *Drosophila* photo-taxis, odor-taxis, and multi-sensory integration. *eLife*, page e06229.

Gerber, B. (2007). The *Drosophila* larva as a model for studying chemosensation and chemosensory learning: a review. *Chemical Senses*, 32(1):65–89.

Gershow, M., Berck, M., Mathew, D., Luo, L., Kane, E. A., Carlson, J. R., and Samuel, A. D. (2012). Controlling airborne cues to study small animal navigation. *Nature methods*, 9(3):290–296.

Gomez-Marin, A., Stephens, G. J., and Louis, M. (2011). Active sampling and decision making in *Drosophila* chemotaxis. *Nature communications*, 2:441.

Gouwens, N. W. and Wilson, R. I. (2009). Signal propagation in *Drosophila* central neurons. *The Journal of Neuroscience*, 29(19):6239–6249.

H.-H.Li, Kroll, J. R., Lennox, S. M., Ogundeyi, O., Jeter, J., Depasquale, G., and Truman, J. W. (2014). A gal4 driver resource for developmental and behavioral studies on the larval cns of *Drosophila*. *Cell Reports*, page In press.

Haddad, R., Khan, R., Takahashi, Y. K., Mori, K., Harel, D., and Sobel, N. (2008). A metric for odorant comparison. *Nature methods*, 5(5):425–429.

Haddad, R., Weiss, T., Khan, R., Nadler, B., Mandairon, N., Bensafi, M., Schneidman, E., and Sobel, N. (2010). Global features of neural activity in the olfactory system form a parallel code that predicts olfactory behavior and perception. *The Journal of Neuroscience*, 30(27):9017–9026.

Heisenberg, M., Borst, A., Wagner, S., and Byers, D. (1985). Drosophila mushroom body mutants are deficient in olfactory learning: Research papers. *Journal of neurogenetics*, 2(1):1–30.

Hernandez-Nunez, L., Belina, J., Klein, M., Si, G., Claus, L., Carlson, J. R., and Samuel, A. D. (2015). Reverse-correlation analysis of navigation dynamics in *Drosophila* larva using optogenetics. *eLife*, page e06225.

Kim, A. J., Lazar, A. A., and Slutskiy, Y. B. (2015). Projection neurons in *Drosophila* antennal lobes signal the acceleration of odor concentrations. *eLife*, page e06651.

Kreher, S. A., Mathew, D., Kim, J., and Carlson, J. R. (2008). Translation of sensory input into behavioral output via an olfactory system. *Neuron*, 59(1):110–124.

Liang, L., Li, Y., Potter, C. J., Yizhar, O., Deisseroth, K., Tsien, R. W., and Luo, L. (2013). Gabaergic projection neurons route selective olfactory inputs to specific higher-order neurons. *Neuron*, 79(5):917–931.

Linster, C. and Smith, B. H. (1997). A computational model of the response of honey bee antennal lobe circuitry to odor mixtures: overshadowing, blocking and unblocking can arise from lateral inhibition. *Behavioural brain research*, 87(1):1–14.

Liu, W. W. and Wilson, R. I. (2013). Glutamate is an inhibitory neurotransmitter in the *Drosophila* olfactory system. *Proceedings of the National Academy of Sciences*, 110(25):10294–10299.

Louis, M., Huber, T., Benton, R., Sakmar, T., and Vosshall, L. (2008). Bilateral olfactory sensory input enhances chemotaxis behavior. *Nature Neuroscience*, 11(2):187–99.

Luo, S. X., Axel, R., and Abbott, L. (2010). Generating sparse and selective third-order responses in the olfactory system of the fly. *Proceedings of the National Academy of Sciences*, 107(23):10713–10718.

Manning, L., Heckscher, E. S., Purice, M. D., Roberts, J., Bennett, A. L., Kroll, J. R., Pollard, J. L., Strader, M. E., Lupton, J. R., Dyukareva, A. V., et al. (2012). A resource for manipulating gene expression and analyzing cis-regulatory modules in the *Drosophila* cns. *Cell reports*, 2(4):1002–1013.

Masuda-Nakagawa, L. M., Gendre, N., O'Kane, C. J., and Stocker, R. F. (2009). Localized olfactory representation in mushroom bodies of *Drosophila* larvae. *Proceedings of the National Academy of Sciences*, 106(25):10314–10319.

Mathew, D., Martelli, C., Kelley-Swift, E., Brusalis, C., Gershow, M., Samuel, A. D., Emonet, T., and Carlson, J. R. (2013). Functional diversity among sensory receptors in a *Drosophila* olfactory circuit. *Proceedings of the National Academy of Sciences*, 110(23):E2134–E2143.

Montague, S. A., Mathew, D., and Carlson, J. R. (2011). Similar odorants elicit different behavioral and physiological responses, some supersustained. *The Journal of Neuroscience*, 31(21):7891–7899.

Nagayama, S., Takahashi, Y. K., Yoshihara, Y., and Mori, K. (2004). Mitral and tufted cells differ in the decoding manner of odor maps in the rat olfactory bulb. *Journal of neurophysiology*, 91(6):2532–2540.

Nagel, K. I., Hong, E. J., and Wilson, R. I. (2015). Synaptic and circuit mechanisms promoting broadband transmission of olfactory stimulus dynamics. *Nature neuroscience*, 18(1):56–65.

Nern, A., Pfeiffer, B. D., and Rubin, G. M. (2015). Optimized tools for multicolor stochastic labeling reveal diverse stereotyped cell arrangements in the fly visual system. *Proceedings of the National Academy of Sciences*, page 201506763.

Ohyama, T., Schneider-Mizell, C. M., Fetter, R. D., Aleman, J. V., Franconville, R., Rivera-Alba, M., Mensh, B. D., Branson, K. M., Simpson, J. H., Truman, J. W., Cardona, A., and Zlatic, M. (2015a). A multilevel multimodal circuit enhances action selection in drosophila. *Nature*.

Ohyama, T., Schneider-Mizell, C. M., Fetter, R. D., Aleman, J. V., Francoville, R., Alba, M. R., Mensh, B. D., Branson, K. M., Simpson, J. H., Truman, J. W., Cardona, A., and Zlatic, M. (2015b). A multilevel multimodal circuit enhances action selection in *Drosophila*. *Nature*, In press.

Okada, R., Awasaki, T., and Ito, K. (2009). Gamma-aminobutyric acid (gaba)-mediated neural connections in the drosophila antennal lobe. *Journal of Comparative Neurology*, 514(1):74–91.

Olsen, S. R., Bhandawat, V., and Wilson, R. I. (2010). Divisive normalization in olfactory population codes. *Neuron*, 66(2):287–299.

Olsen, S. R. and Wilson, R. I. (2008). Lateral presynaptic inhibition mediates gain control in an olfactory circuit. *Nature*, 452(7190):956–960.

Otsu, N. (1975). A threshold selection method from gray-level histograms. *Automatica*, 11(285-296):23–27.

Prieto-Godino, L. L., Diegelmann, S., and Bate, M. (2012). Embryonic origin of olfactory circuitry in drosophila: contact and activity-mediated interactions pattern connectivity in the antennal lobe. *PLoS Biology*.

Python, F. and Stocker, R. (2002). Adult-like complexity of the larval antennal lobe of *Dr. melanogaster* despite markedly low numbers of odorant receptor neurons. *Cell Tissue Res*, 445(4):374–87.

Rall, W., Shepherd, G., Reese, T., and Brightman, M. (1966). Dendrodendritic synaptic pathway for inhibition in the olfactory bulb. *Experimental neurology*, 14(1):44–56.

Ramaekers, A., Magenat, E., Marin, E., Gendre, N., Jefferis, G., Luo, L., and Stocker, R. (2005). Glomerular Maps without Cellular Redundancy at Successive Levels of the *Drosophila* Larval Olfactory Circuit. *Current Biology*, 15(11):982–92.

Ressler, K. J., Sullivan, S. L., and Buck, L. B. (1994). Information coding in the olfactory system: evidence for a stereotyped and highly organized epitope map in the olfactory bulb. *Cell*, 79(7):1245–1255.

Roy, B., Singh, A. P., Shetty, C., Chaudhary, V., North, A., Landgraf, M., Vijayraghavan, K., and Rodrigues, V. (2007). Metamorphosis of an identified serotonergic neuron in the *Drosophila* olfactory system. *Neural Dev*, 2:20.

Saalfeld, S., Cardona, A., Hartenstein, V., and Tomancak, P. (2009). CATMAID: Collaborative Annotation Toolkit for Massive Amounts of Image Data. *Bioinformatics*, 25(19):1984–1986.

Satou, M. (1992). Synaptic organization of the olfactory bulb and its central projection. In *Fish Chemoreception*, pages 40–59. Springer.

Schneider-Mizell, C. M., Gerhard, S., Longair, M., Kazimiers, T., Li, F., Zwart, M. F., Champion, A., Midgley, F., Fetter, R., Saalfeld, S., et al. (2015). Quantitative neuroanatomy for connectomics in drosophila. *bioRxiv*, page 026617.

Schulze, A., Gomez-Marin, A., Rajendran, V. G., Lott, G., Musy, M., Ahammad, P., Deogade, A., Sharpe, J., Riedl, J., Jarriault, D., et al. (2015). Dynamical feature extraction at the sensory periphery guides chemotaxis. *eLife*, 4:e06694.

Selcho, M., Pauls, D., el Jundi, B., Stocker, R. F., and Thum, A. S. (2012). The role of octopamine and tyramine in *Drosophila* larval locomotion. *Journal of Comparative Neurology*, 520(16):3764–3785.

Selcho, M., Pauls, D., Huser, A., Stocker, R. F., and Thum, A. S. (2014). Characterization of the octopaminergic and tyraminergic neurons in the central brain of *Drosophila* larvae. *Journal of Comparative Neurology*, 522(15):3485–3500.

Sosulski, D. L., Bloom, M. L., Cutforth, T., Axel, R., and Datta, S. R. (2011). Distinct representations of olfactory information in different cortical centres. *Nature*, 472(7342):213–216.

Stocker, R., Lienhard, M., Borst, A., and Fischbach, K. (1990). Neuronal architecture of the antennal lobe in *Drosophila* melanogaster. *Cell and tissue research*, 262(1):9–34.

Su, C.-Y., Menuz, K., and Carlson, J. R. (2009). Olfactory perception: receptors, cells, and circuits. *Cell*, 139(1):45–59.

Thum, A. S., Leisibach, B., Gendre, N., Selcho, M., and Stocker, R. F. (2011). Diversity, variability, and suboesophageal connectivity of antennal lobe neurons in d. melanogaster larvae. *Journal of Comparative Neurology*, 519(17):3415–3432.

Vogelstein, J. T., Park, Y., Ohyama, T., Kerr, R. A., Truman, J. W., Priebe, C. E., and Zlatic, M. (2014). Discovery of brainwide neural-behavioral maps via multiscale unsupervised structure learning. *Science*, 344(6182):386–392.

Vosshall, L. and Stocker, R. (2007). Molecular architecture of smell and taste in *Drosophila*. *Annu Rev Neurosci*, 30:505–33.

Vosshall, L. B., Wong, A. M., and Axel, R. (2000). An olfactory sensory map in the fly brain. *Cell*, 102(2):147–159.

Wang, F., Nemes, A., Mendelsohn, M., and Axel, R. (1998). Odorant receptors govern the formation of a precise topographic map. *Cell*, 93(1):47–60.

Wilson, R. and Laurent, G. (2005). Role of GABAergic inhibition in shaping odor-evoked spatiotemporal patterns in *Drosophila* antennal lobe. *J Neurosci*, 25:9069–79.

Wong, A., Wang, J., and Axel, R. (2002). Spatial Representation of the Glomerular Map in the *Drosophila* Protocerebrum. *Cell*, 109:229–41.

Yaksi, E. and Wilson, R. (2010). Electrical coupling between olfactory glomeruli. *Neuron*, 67:1034–47.

Zhu, P., Frank, T., and Friedrich, R. W. (2013). Equalization of odor representations by a network of electrically coupled inhibitory interneurons. *Nature neuroscience*, 16(11):1678–1686.

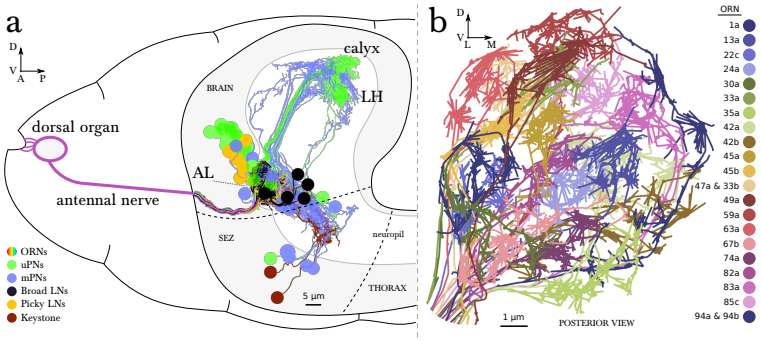

c

Right antennal lobe	ORN (21)	uPN (21)	mPN (14)	SEZ neurons (6)	Broad LN Trio (3)	Broad LN Duet (2)	Keystone	Choosy LN (2)	Ventral LN	Picky 0 LN	Picky 1-4 LN (4)
ORN (21)	0	58	23	14	44	65	38	35	38	67	52
uPN (21)	0	2	5	1	21	11	11	9	6	4	3
mPN (14)	0	1	3	0	1	1	0	3	1	0	1
SEZ neurons (6)	0	0	1	1	1	0	0	1	1	0	0
Broad LN Trio (3)	46	7	4	1	14	6	12	6	7	4	6
Broad LN Duet (2)	28	16	5	0	2	3	1	5	3	9	4
Keystone(2)	17	2	2	1	5	1	0	5	0	2	4
Choosy LN (2)	1	6	2	3	0	2	0	3	0	1	2
Ventral LN	0	1	1	1	1	1	1	4	0	2	3
Picky 0 LN	5	2	1	0	1	1	8	2	4	0	3
Picky 1-4 LN (4)	1	2	13	6	1	2	1	8	4	0	3
TOTAL	99	96	58	28	90	93	72	79	64	90	79

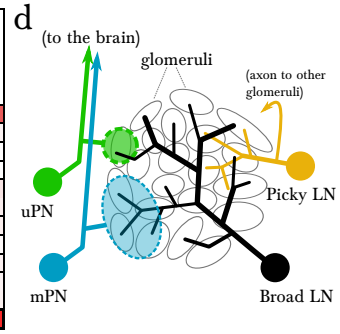

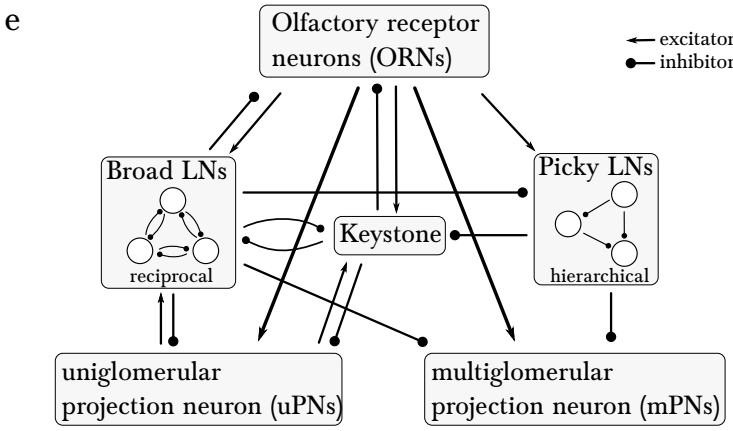

Figure 1: **Overview of the wiring diagram of the glomerularly organized olfactory system of the larval *Drosophila*. A** Schematic of the olfactory system of the larval *Drosophila* with EM-reconstructed skeletons overlaid. The ORN cell bodies are housed in the dorsal organ ganglion, extend dendrites into the dorsal organ, and emit axons to the brain via the antennal nerve. Like in all insects, neuron cell bodies (circles) reside in the outer layer of the nervous system (grey), and project their arbors into the neuropil (white) where they form synapses. Also shown are the major classes of local neurons (Broad LNs, Picky LNs and Keystone) and the 2 classes of projection neurons. The arbors of the Broad LNs (black) specifically innervate the AL. LNs and mPN dendrites can extend into the subesophageal zone (SEZ), innervated by sensory neurons of other modalities. uPNs project to specific brain areas (mushroom body calyx and lateral horn; LH), and mPNs mostly project to other nearby brain areas. **B** The larva presents 21 unique olfactory glomeruli, each defined by a single ORN expressing a single or a unique pair of olfactory receptors. We reconstructed each ORN with a skeleton and annotated its synapses, here colored like the skeleton to better illustrate each glomerulus. See suppl. fig. 1 for individual renderings that aided in the identification of each unique ORN. **C** Summary connectivity table for the right antennal lobe with all major neuron classes (only missing the 4 neuromodulatory neurons and the descending neuron from the brain), indicating the percent of postsynaptic sites of a column neuron contributed by a row neuron. For most neurons, the vast majority of their inputs originate in other neurons within the antennal lobe. In parentheses, the number of neurons that belong to each cell type. We show only connections with at least two synapses, consistently found among homologous identified neurons in both the left and right antennal lobes. Percentages between 0 and 0.5 are rounded down to 0. **D** Schematic of the innervation patterns of the main classes of LNs and PNs in the antennal lobe. White ovals represent the glomeruli. Solid circles are cell bodies. Shaded areas with dotted outlines represent the extent of the PN dendritic arbors, with each uPN (green) innervating one glomerulus and each mPN (blue) innervating multiple glomeruli. Their axons (arrows) project to the brain. Broad LNs (black) are axonless and present panglomerular arbors. Picky LNs (orange) dendrites span multiple glomeruli and their axons (arrow; not shown) target a different yet overlapping set of glomeruli as well as regions outside the olfactory system. Choosy LNs (not shown) are similar to Picky LNs. **E** A simplified wiring diagram of the larval olfactory system with only the main connections. ORNs are excitatory. All shown LNs are inhibitory. Broad LNs reciprocally connect to all glomeruli and each other and thus engage in presynaptic inhibition (on ORNs) and postsynaptic inhibition (on uPNs). Picky LNs form a hierarchical circuit and selectively synapse onto mPNs. Another LN, Keystone, receives inputs from ORNs, one Picky LN and non-ORN sensories, and can alter the operational mode of the entire olfactory system by altering the pattern of inhibition (see text).

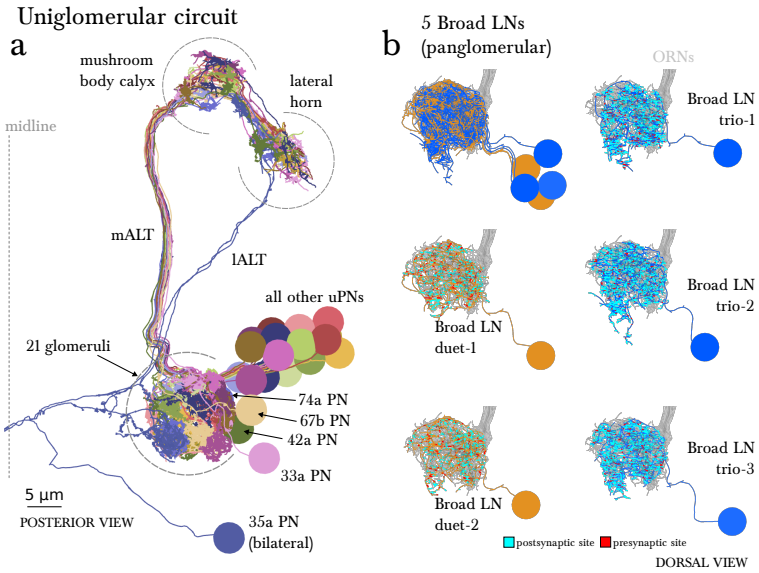

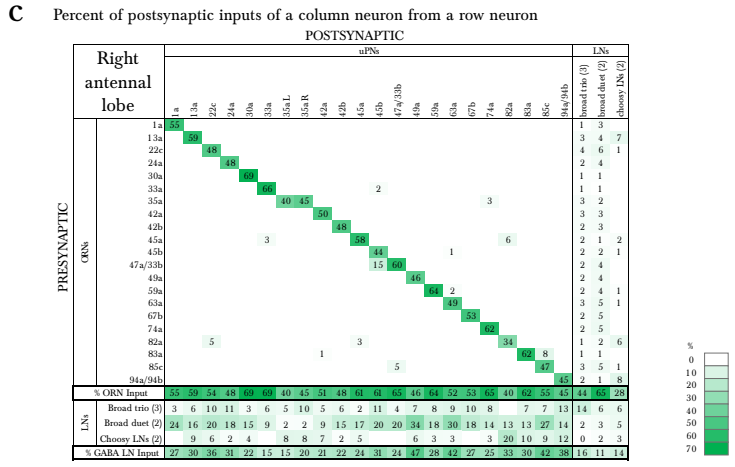

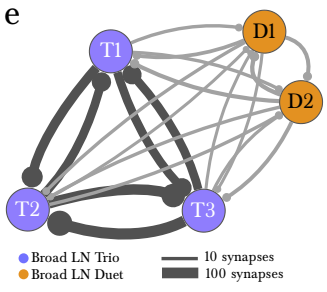

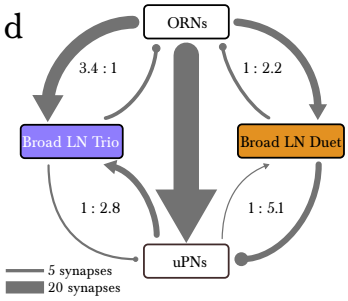

Figure 2: **The uniglomerular circuit consists of 21 glomerular-specific projection neurons, which interact primarily with their corresponding ORN and with the 5 panglomerular LNs (Broad LNs), each an identified neuron. A** Posterior view of the EM-reconstructed uPNs of the right antennal lobe. The dendrites of each uPN delineate the glomerular boundaries, and the axons project to both the mushroom body (learning and memory center) and the lateral horn (innate center). 19 uPNs are likely generated by the same neuroblast lineage BAmv3 (Das et al., 2013) (although the uPNs for 42a, 74a, and 67b are slightly separated from the rest), and the other two (the uPNs for 33a and 35a) clearly derive from two other neuroblasts. Note that the 35a uPN is bilateral, ascends through a different tract, and receives additional inputs outside of the antennal lobe. The 33a uPN does not synapse within the calyx and the 82a uPN does not continue to the lateral horn. The left antennal lobe (not shown) is a mirror image of the right one. **B** Dorsal view of the EM-reconstructed, axonless Broad LNs (duet in orange; trio in blue) shown together and individually. All neurons are on the same lineage: BAlc (Das et al., 2013). The pre-(red) and post-(cyan) synaptic sites on these panglomerular neurons are fairly uniformly distributed. ORNs in grey for reference. These neurons extend posteriorly out of the olfactory glomeruli to receive synapses from 2 non-ORN sensory neurons that enter the brain via the antennal nerve. **C** Percentage of the total number of postsynaptic sites on the dendrite of an uPN, Broad LN or Choosy LN (columns) that originate in a given ORN or LN (rows) for the right antennal lobe. Since the 35a uPN is bilateral, we include inputs to it from both antennal lobes. We show only connections with at least two synapses, consistently found among homologous identified neurons in both the left and right antennal lobes. Percentages between 0 and 1 are rounded to 1, but totals are computed from raw numbers. The uniglomerular nature of uPNs (notice the green diagonal) and panglomerular nature of Broad LNs is evident. The Broad LN duet generally contributes more synapses onto uPNs than the Broad LN trio does. While the number of synapses that an ORN makes onto its uPN varies widely (24-120 synapses; see suppl. adjacency matrix), this number is tailored to the size of the target uPN dendrite given that percentage of inputs the ORN contributes to the uPN is much less varied (mostly 45-65%). For an extended version of this table that includes all LNs, see supp. fig. 2. **D** Both Broad LN types (trio and duet) mediate presynaptic inhibition (synapses onto ORN axons) similarly, but the duet shows far stronger postsynaptic inhibition (synapses onto uPN dendrites) while the trio receives far more dendro-dendritic synapses from uPNs. Connections among Broad LNs are not shown for simplicity. Each arrow is weighted linearly for the number of synapses for an average single Broad LN of each type. **E** The 5 Broad LNs that govern this circuit synapse reciprocally, with the trio type synapsing more strongly onto each other. Shown here for the right antennal lobe with arrow thickness weighted by the square root of the number of synapses.

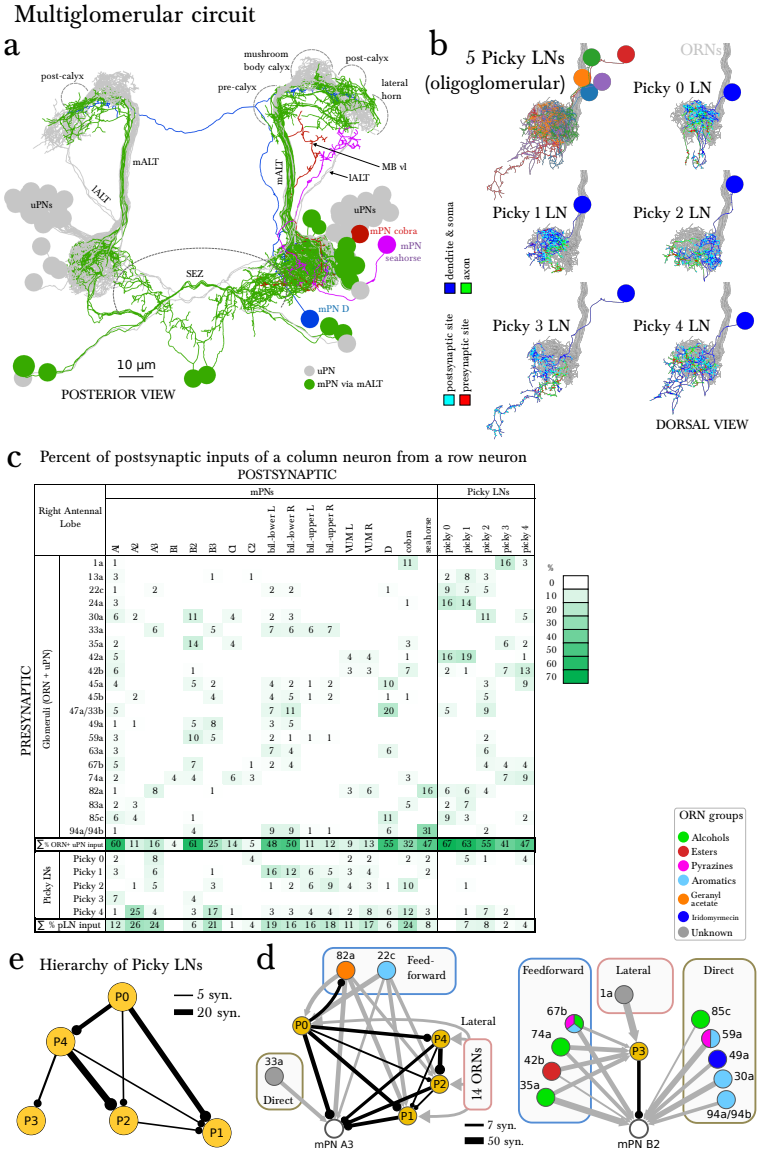

Figure 3: **The multiglomerular circuit consists of 14 mPNs that project to the brain and 5 Picky LNs, each an identified neuron. A** Posterior view of EM-reconstructed mPNs that innervate the right antennal lobe (in color; uPNs in grey for reference), each receiving inputs from a subset of olfactory glomeruli but many also from non-ORN sensory neurons in the subesophageal zone (SEZ). Most mPNs (green) project via the same tract as the uPNs (mALT). They can project via other tracts (other colors), but never the mlALT used by the iPNs of the adult *Drosophila*. The mPNs project to many regions including a pre-calyx area, a post-calyx area, the lateral horn (LH) and the mushroom body vertical lobe (MB vl). mPNs are generated by diverse neuroblast lineages including BAlp4, BAla1, and others (Das et al., 2013). **B** Dorsal view of the EM-reconstructed Picky LNs shown together and individually. When shown individually, the Picky LNs are in 2 colors: blue for the dendrites and soma, and green for the axon. Zoom in to observe that presynaptic sites (red) are predominantly on the axon, whereas postsynaptic sites (cyan) are mostly on dendrites. Collectively, the dendritic arbors of the 5 Picky LNs tile the olfactory glomeruli. The dendrites of the picky 3 and 4 extend significantly into the SEZ. They all originate from the same neuroblast lineage: BAla2 (Das et al., 2013). **C** Percentage of the total number of postsynaptic sites on the dendrite of a mPN or Picky LN (column neuron) that originate from a given glomerulus or Picky LN (row neurons). Here we define the glomerulus as connections from the ORN or via dendro-dendritic synapses from a given ORN's uPN. This is most relevant for mPN A1, which can receive more synapses from an ORN's uPN than the ORN itself (see suppl. Adjacency Matrix). We show the inputs to the mPNs and Picky LNs for the right antennal lobe, but for all bilateral mPNs (bil.-lower, bil.-upper, and VUM) we include inputs from both sides. We show only connections with at least two synapses, consistently found among homologous identified neurons in both the left and right antennal lobes. Percentages between 0 and 1 are rounded to 1, but totals are computed from raw numbers. Connections in this table are stereotyped (when comparing the left and right antennal lobes) and selective. Note that mPNs that receive many inputs from non-ORN sensory neurons in the SEZ have a low total of ORN+uPN input. For an extended version of this table that includes all LNs see supp. fig. 2. **D** The direct upstream connectivity for two mPNs, with ORNs colored by the groups emerging from the PCA analysis of odor tuning. Connections from ORNs and Picky LNs to mPNs create 3 different types of motifs: *direct* excitatory connections from ORNs, *lateral* inhibitory connections from ORNs only via Picky LNs, and *feedforward loops* where an ORN connects both directly to the mPN and laterally through a Picky LN. Note the activity of Picky LN 0 could alter the integration function of for mPN A3 and indirectly for B2, as well as many other mPNs (not shown). Arrow thicknesses are weighted by the square root of the number of synapses between neurons. **E** The Picky LN hierarchy, dominated by Picky LN 0, here showing connections with 2 or more consistent synapses between bilaterally homologous neurons. Some of these connections are axo-axonic (see suppl. fig. 3).

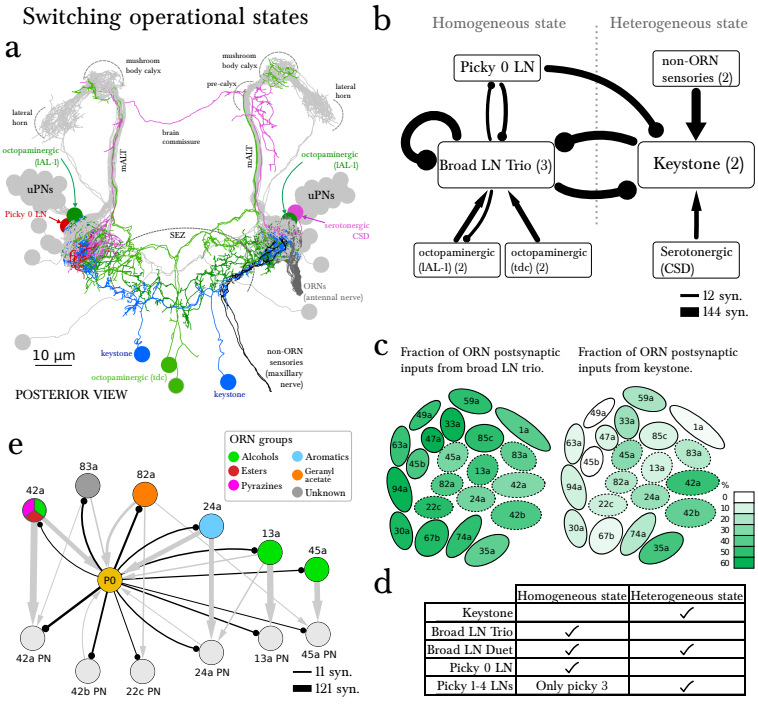

	Homogeneous state	Heterogeneous state
Keystone		✓
Broad LN Trio	✓	
Broad LN Duet	✓	✓
Picky 0 LN	✓	
Picky 1-4 LNs	Only picky 3	✓

Figure 4: **The wiring diagram suggests two operational states: homogeneous or heterogeneous presynaptic inhibition. A** Posterior view of the EM-reconstructed neurons innervating the left antennal lobe that could govern the switch (uPNs in grey and right ORNs in dark grey for reference). The Keystone LN (blue) has a symmetric bilateral arbor and additionally innervates the SEZ, receiving inputs from non-ORN sensory neurons (in black). Neuromodulatory neurons that make direct morphological synapses onto LNs are serotonergic (CSD in pink; projects contralaterally after collecting inputs from near the MB calyx) and octopaminergic (lAL-1 and two tdc, in dark and light green), and all arborize well beyond the antennal lobe. Also included is Picky LN 0 (red). **B** A wiring diagram outlining the strong LN-LN connections, showing the core reciprocal inhibition between Broad LN trio and Keystone that could mediate the switch between homogeneous (panglomerular) presynaptic inhibition and heterogenous (selective) presynaptic inhibition. For simplicity, neurons are grouped together if they belong to the same neuron type, with the number of neurons belonging to each group indicated in parentheses. Connections are weighted by the square root of the number of synapses between groups of neurons. The self-arrow for the Broad LN trio represents the average number of synapses that one of the trio neurons receives from the other two. Picky LN 0 inhibits Keystone, therefore disinhibiting the Broad LN trio and promoting homogeneous presynaptic inhibition. The maxillary nerve sensory neurons are the top input providers of Keystone and may drive the system towards heterogeneous presynaptic inhibition (see **C**). The effect of direct inputs from neuromodulatory neurons is unknown, but at least it has been suggested that octopaminergic neurons may have an excitatory effect on inhibitory LNs (Linster and Smith, 1997). **C** Cartoon of glomeruli colored by the percentage of inputs onto ORN axon terminals provided by the Broad LN trio and from Keystone, indicating the amount of presynaptic inhibition (onto ORNs) in either state. The inhibition provided by Broad LN trio is much more uniform than the inhibition provided by Keystone. Dotted lines indicate glomeruli that receive Picky LN 0 input on either the ORN or uPN. **D** The LNs putatively active in each state. **E** Unlike other Picky LNs, picky 0 makes synapses onto ORN axon terminals and many uPNs. Here connections with 2 or more synapses consistent between bilaterally homologous neuron pairs are shown. Arrow thicknesses are weighted by the square root of the number of synapses between neurons. With the exception of 45a, all shown ORNs and uPNs belong to glomeruli that synapse onto Picky LN 0 as well. Thus Picky LN 0 provides both pre- and postsynaptic inhibition to a small set of glomeruli.

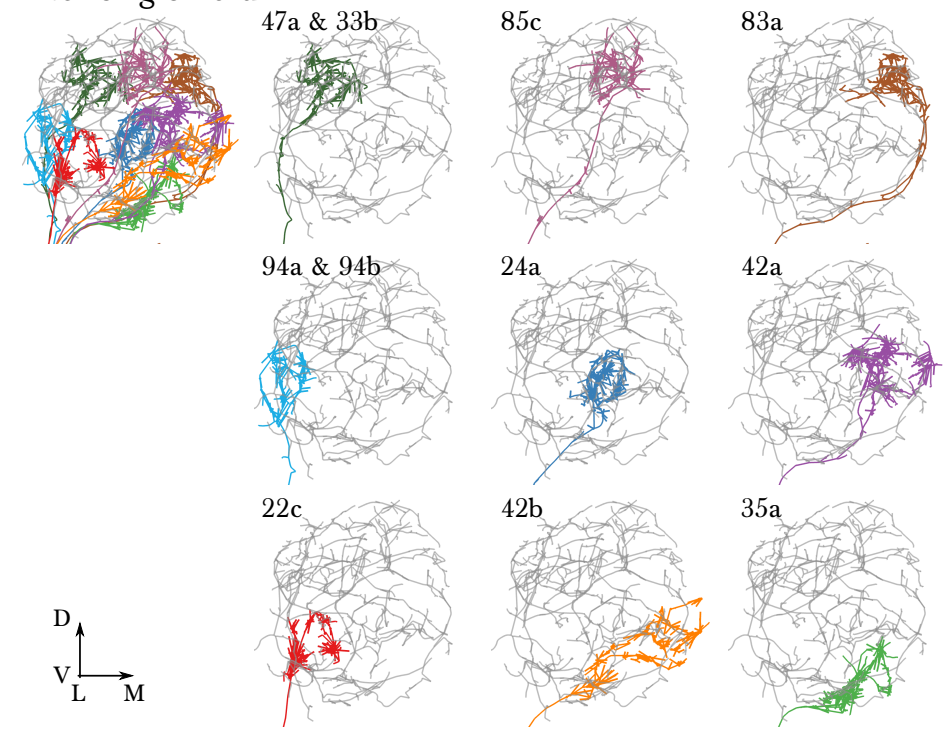

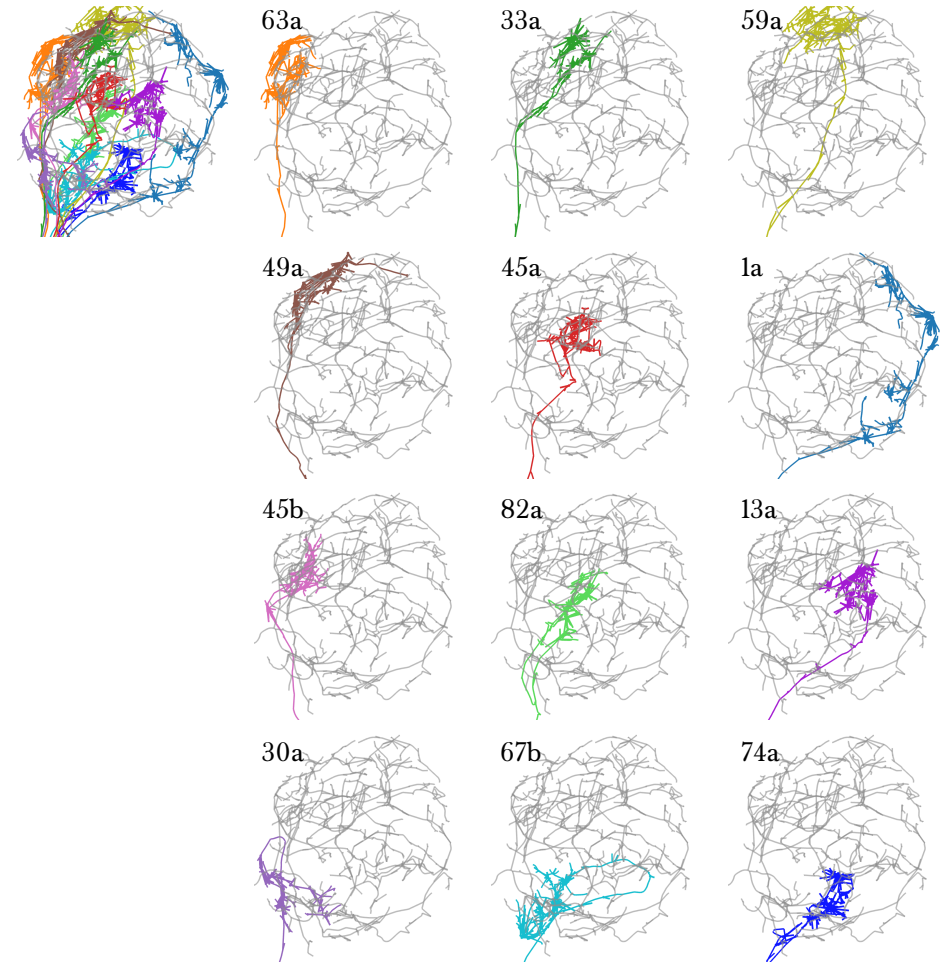

Supplementary Figure 1: **A single, identified ORN for each glomerulus in the antennal lobe of the first instar larva.** Each panel shows an EM-reconstructed arbor of an ORN (colored) over the background of a Broad LN Duet (grey). ORN synapses are rendered in the same color as the skeleton. To the left, all ORNs of each half of the antennal lobe are rendered together. The orientation (lateral to the left, dorsal up) and relative position of each ORN has been chosen to exactly match the arrangement in the supplementary figure 1 of Masuda-Nagakawa et al. 2009, where each individual ORN was identified and labeled with GFP using genetic driver lines.

Right Antennal Lobe		uPNs																							LNs												
		1a	13a	22c	24a	30a	33a	35a L	35a R	42a	42b	45a	45b	47a/33b	49a	59a	63a	67b	74a	82a	83a	85c	94a/94b	broad trio (3)	broad duet (2)	keystone (2)	choosy LNs (2)	ventral LN	picky 0	picky 1	picky 2	picky 3	picky 4
ORNs	1a	55																						1	3								16	3
	13a		59																					3	4	2	7	29	2	7	3			
	22c			48																				4	6	2	1		9	5	4			
	24a				48																			2	4	3		6	16	14				
	30a					69																		1	1	2					11			4
	33a						66						2											1	1									
	35a							40	45										3					3	2	4							6	2
	42a									50														3	3	4			16	18				1
	42b										48													2	3	3			2	1			7	10
	45a						3					58								6				2	1	2	2				3			9
	45b												44					1						2	2		1				5			
	47a/33b												15	60										2	4	1			5		9			
	49a														46									2	4									
	59a															64	2							2	4	2	1				2			
	63a																49							3	5	1	1				5			
	67b																	53						2	5	2							4	3	4
	74a																		62					2	5	4								7	9
	82a			5								3								34				1	2	2	6		6	6	4			
	83a									1											62	8		1	1	1			2	7				
	85c													5								47		3	5	1	1		7	3				2
	94a/94b																						45	2	1	2	8				2			
% ORN Input		55	59	54	48	69	69	40	45	51	48	61	61	65	46	64	52	53	65	40	62	55	45	44	65	38	28	35	64	62	53	39	42
LNs	broad trio (3)	3	6	10	11	3	6	5	10	5	6	2	11	4	7	8	9	10	8		7	7	13	14	6	12	6	7	4	7	4	8	3
	broad duet (2)	24	16	20	18	15	9	2	2	9	15	17	20	20	34	18	30	18	14	13	13	27	14	2	3	1	5	3	9	5	4	4	2
	keystone (2)				5			2	1	10	11					3					2		1	5	1		5		2	6	4	1	2
	choosy LNs (2)		9	6	2	4		8	8	7	2	5			6	3	3		3	20	10	9	12		2		3		1	4	1		2
	ventral LN		4		2					2	1								4					1	1	1	4		2	3	6		4
	picky 0		4	2	5					7	5	2												1	1	8	2	4		5	1		4
	picky 1		1																						1	1	2						
	picky 2																										1			1			
	picky 3																	9									2						
	picky 4							1	7			4								4	1				1		3	4		1	7	2		
% LN Input		27	39	38	43	22	15	18	28	39	39	31	31	24	47	31	42	37	29	37	34	42	39	22	16	22	32	17	19	31	27	15	18
% ORN+LN Input		82	98	92	91	92	84	58	73	91	88	92	91	89	93	95	94	89	94	77	96	97	85	66	81	60	59	51	83	93	80	54	60
Desc. and Modulatory	Descending						3																				1				1	1		
	CSD (2)						1																		1	3							1	1
	IAL-1 (2)							1	1									1						2	1		1	5	2				3	1
	tdc (2)																	3						2									1	

Right Antennal Lobe		mPNs																LNs										
		A1	A2	A3	B1	B2	B3	C1	C2	bil.-lower L	bil.-lower R	bil.-upper L	bil.-upper R	VUM L	VUM R	D	cobra	seahorse	broad trio (3)	broad duet (2)	keystone (2)	choosy LNs (2)	ventral LN	picky 0	picky 1	picky 2	picky 3	picky 4
Glomeruli (ORN+uPN)	1a	1															11		1	3							16	3
	13a	3					1		1										4	4	3	7	34	2	8	3		
	22c	1		2						2	2					1			5	7	3	1		9	5	5		
	24a	3															1		4	4	4	1	6	16	14			
	30a	6	2			11		4		2	3								2	2	2					11		5
	33a			6			5			7	6	6	7						1	1								
	35a	2				14		4									3		3	2	4						6	2
	42a	5												4	4		1		4	4	6			16	19			1
	42b	6				1								3	3		7		4	3	5			2	1		7	13
	45a	4				5	2			4	2	1	2			10			2	1	3	2				3		9
	45b		2				4			4	5	1	2			1	1		3	3		1				5		
	47a/33b	5								7	11					20			3	5	1			5		9		
	49a	1	1			5	8			3	5								3	5		1						
	59a	3				10	5			2	1	1	1						3	4	2	1				2		
	63a	3								7	4					6			4	6	1	2				6		
	67b	5				7			1	2	4								4	6	2	3				4	4	4
	74a	2			4	4		6	3								3		4	6	5						7	9
	82a	1		8			1							3	6			16	1	2	2	6		6	6	4		
	83a	2	3														5		2	2	1			2	7			
	85c	6	4			1										11			5	5	2	2		9	3			2
	94a/94b					4				9	9	1	1			6		31	3	1	3	9				2		
% ORN+uPN input		59	11	16	4	61	25	14	5	48	50	11	12	9	13	55	32	47	64	76	48	37	40	67	63	55	41	47
LNs	broad trio (3)	4	1	2		5	6	1	3	4	5	8	6			7	4	2	14	6	12	6	7	4	7	4	8	3
	broad duet (2)	2	1	2		1	3		7	2	2	22	22	8	6	4	2		2	3	1	5	3	9	5	4	4	2
	keystone (2)				1	3				1	1			1	2	9		6	5	1		5		2	6	4	1	2
	choosy LNs (2)			4	3	6	2		1	1	1	4	8				1			2		3		1	4	1		2
	ventral LN				4	1												7	1	1	1	4		2	3	6		4
	picky 0	2		8					4					2	2		2	2	1	1	8	2	4		5	1		4
	picky 1	3		6			1			16	12	6	5	3	4			2		1	1	2						
	picky 2		1	5			3			1	2	6	9	4	3	1	10					1			1			
	picky 3	7				4																2						
	picky 4		25	4		3	17	1		3	3	4	4	2	8	6	12	3		1		3	4		1	7	2	
% LN Input		18	28	32	8	22	32	3	15	27	25	49	54	20	25	26	31	23	22	16	22	32	17	19	31	27	15	18
% ORN+uPN+LN input		77	39	48	12	84	57	17	20	75	75	61	66	29	38	81	63	69	87	92	70	69	57	86	94	82	56	65
Desc. and Modulatory	Descending		1	2			8	1		6	4	6	1	2	3		2					1			1	1		
	CSD (2)	2			5			1	5							1				1	3						1	1
	IAL-1 (2)		2				1										2		2	1		1	5	2			3	1
	tdc (2)					1		2				1	1	1	2				2								1	

Supplementary Figure 2: **Extended version of tables in fig. 2c and 3c, including all other olfactory-related neurons.** Tables show percent of postsynaptic sites of a column neuron contributed by a row neuron. We show only connections with at least two synapses, consistently found among homologous identified neurons in both the left and right antennal lobes. Percentages between 0 and 0.5 are removed. For bilateral neurons, inputs from both sides are included.

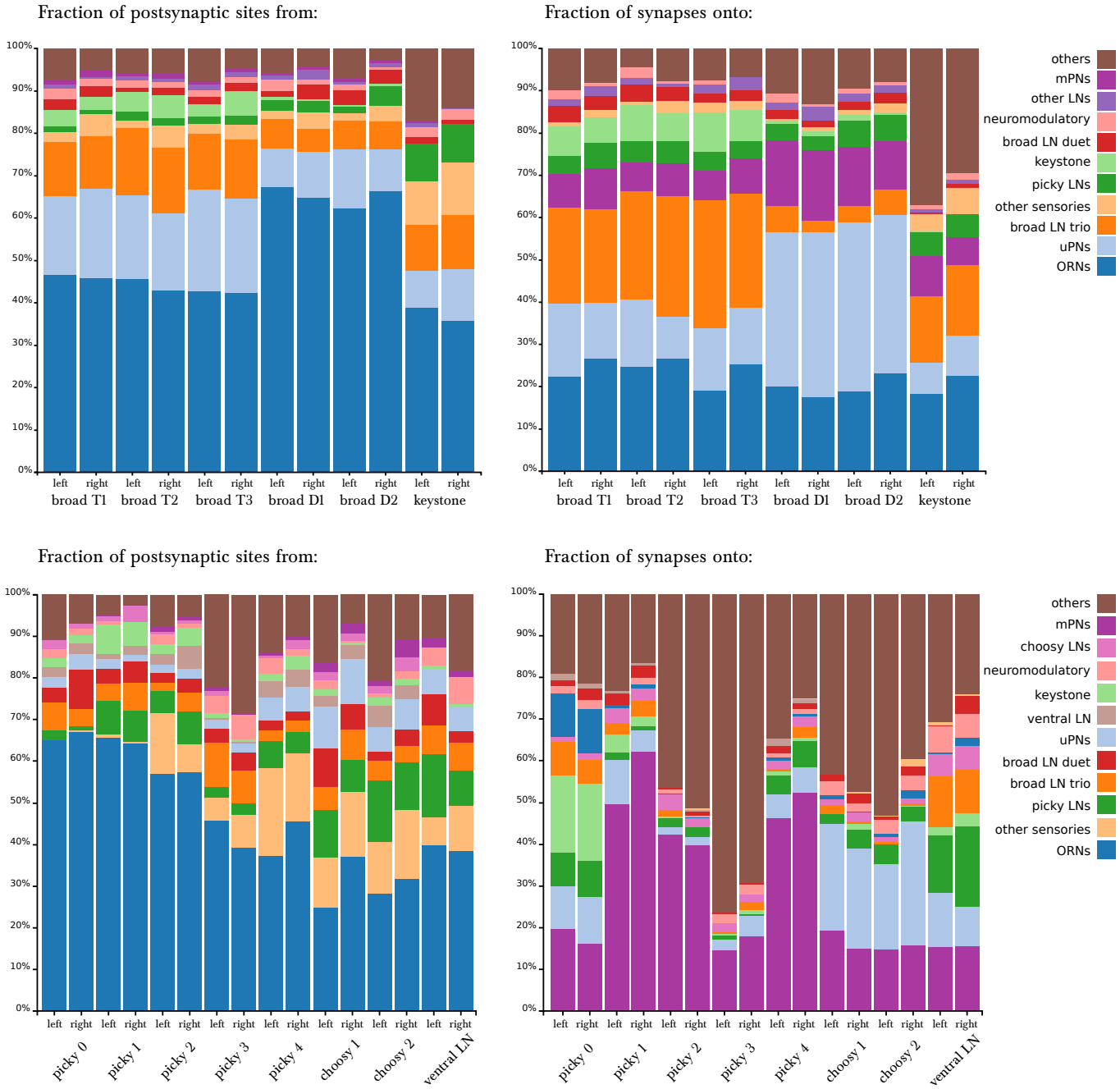

Supplementary Figure 3: **Percentage of synapses of LNs from/onto specific cell types.** The entry for each neuron presents two bars, for the left and right homologs. **Top row**, Broad LNs and keystone. T: Trio, D: Duet. *Left*, differences between the Trio and Duet subtypes are evident in the fraction of inputs that originates in ORNs, uPNs and keystone. The Duet subtype presents a far larger fraction of its inputs from ORNs, and barely receives any inputs from Keystone. By its pattern of inputs, keystone resembles a Broad LN Trio neuron, except for the large fraction of non-ORN inputs and the inputs from Picky LNs (specifically from Picky 0 LN). *Right*, note how the Trio subtype devote about 25% of their synapses to each other, whereas the Duet subtype prefers uPNs the most, providing postsynaptic inhibition to the glomeruli (both lateral and feedforward inhibition). Keystone differs from the Broad LNs in that it targets uPNs much more weakly, preferring instead the Broad LN Trio and a variety of other neurons. **Bottom row**, Picky LNs, Choosy LNs and Ventral LN. *Left*, the fraction of inputs from ORNs stand out as a large difference among Picky LNs, with Picky-3 and -4 receiving substantially fewer, similarly to Choosy LNs. The fraction of inputs received from other Picky LNs (green) is among the most distinguishing feature of Picky-0 LN, which receives close to none. *Right*, in contrast to the similar patterns of inputs onto all Picky LNs, Picky-0 LN stands out as very different from other Picky LNs in its choice of downstream synaptic partners, spreading approximately evenly between ORNs, uPNs, mPNs, other Picky LNs and Keystone. Choosy LNs strongly prefer uPNs, being therefore strong providers of postsynaptic inhibition to glomeruli. Notice that Picky LNs, Choosy LNs and Ventral LN have a larger fraction of synapses to/from "other", with their arbors spreading towards adjacent sensory neuropils in the SEZ.

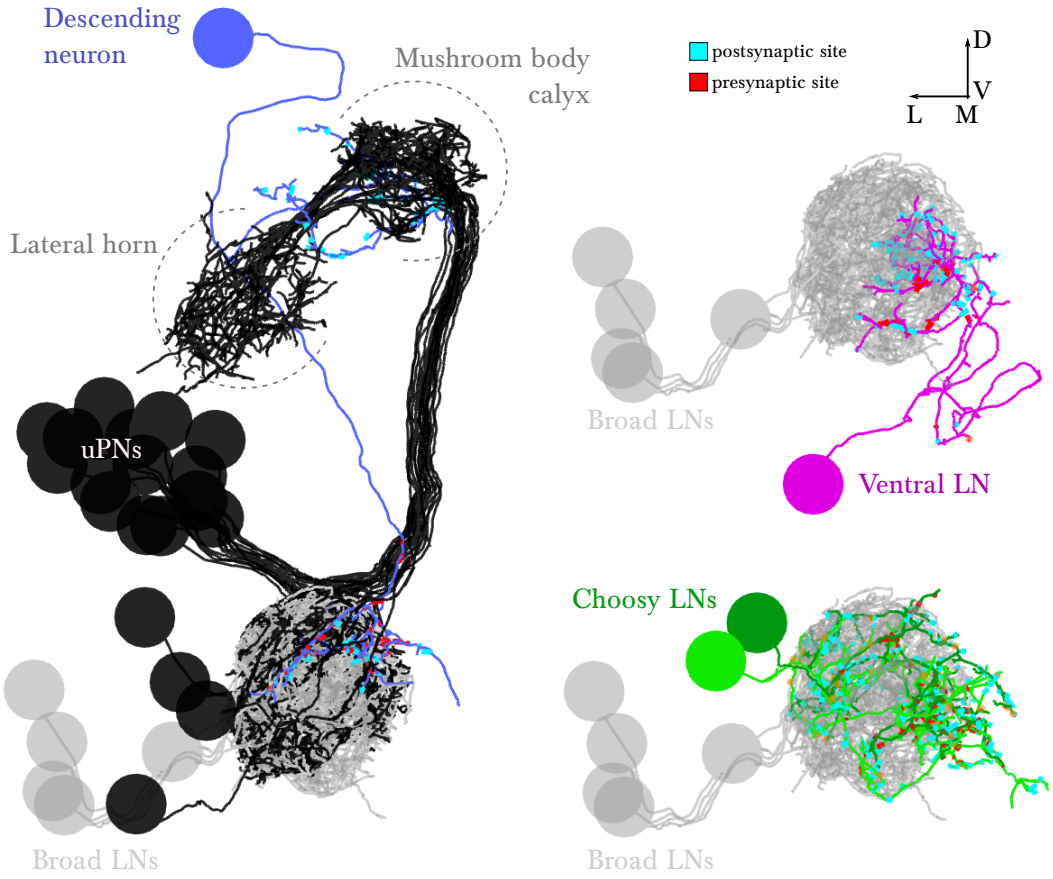

Supplementary Figure 4: **EM-reconstructed arbors of the descending neuron, Choosy LNs and Ventral LN.** Renderings of the left antennal lobe. These 4 identified neurons present similar morphology and connectivity in the right antennal lobe. Posterior view. Broad LNs and uPNs are shown for reference. The morphology, cell body position and number of Choosy LNs matches that of the pair of GABAergic LNs described in fig. 2 L-O of Thum et al., 2011.

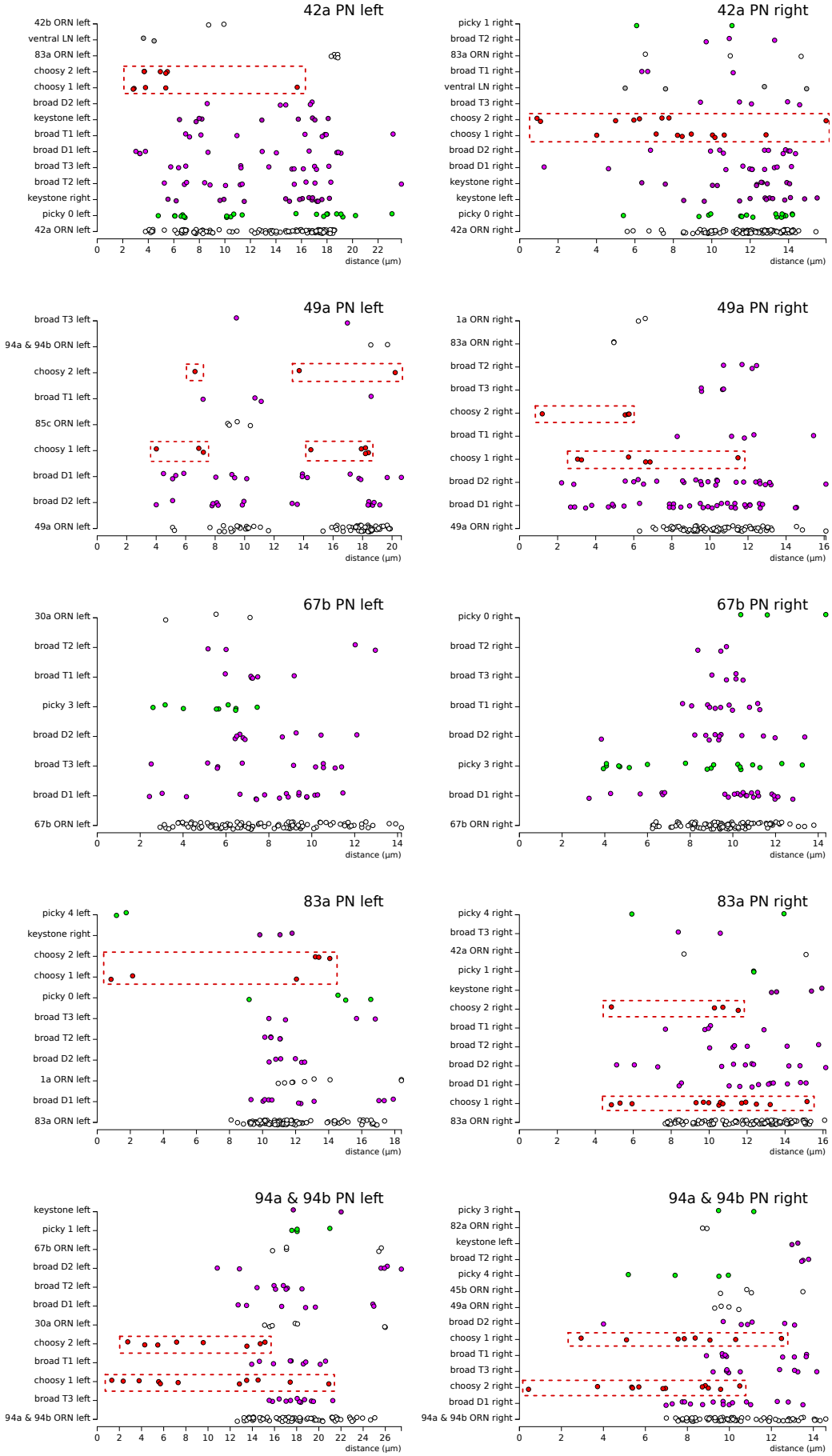

Supplementary Figure 5: **Distribution of postsynaptic sites on the uPN dendrites.** We show 5 examples, plotting the distance (along the cable) of individual postsynaptic sites (colored dots) to the axon initial segment of each uPN. The same type of presynaptic neuron presents the same color across all plots. Notice how Choosy LN inputs (red, framed in a red box) onto uPNs are generally more proximal to the axon initial segment than other inhibitory inputs such as from Broad LNs; particularly noticeable for 42a PN (top row) and 94 & 94b PN (bottom row). No noticeable difference exists between Broad LN Duet and Trio. Notice that the left 49a PN presents an arbor with two main dendrites, with one being further than the other from the axon initial segment, explaining the split in the distribution of distances of postsynaptic sites. While 67b PN (third row) does not receive inputs from Choosy LNs, the Picky LN 3 (light green), which specifically targets 67b PN and no other uPN, provides proximal inputs. Presynaptic neurons are ordered with the largest contributor at the bottom of each plot.

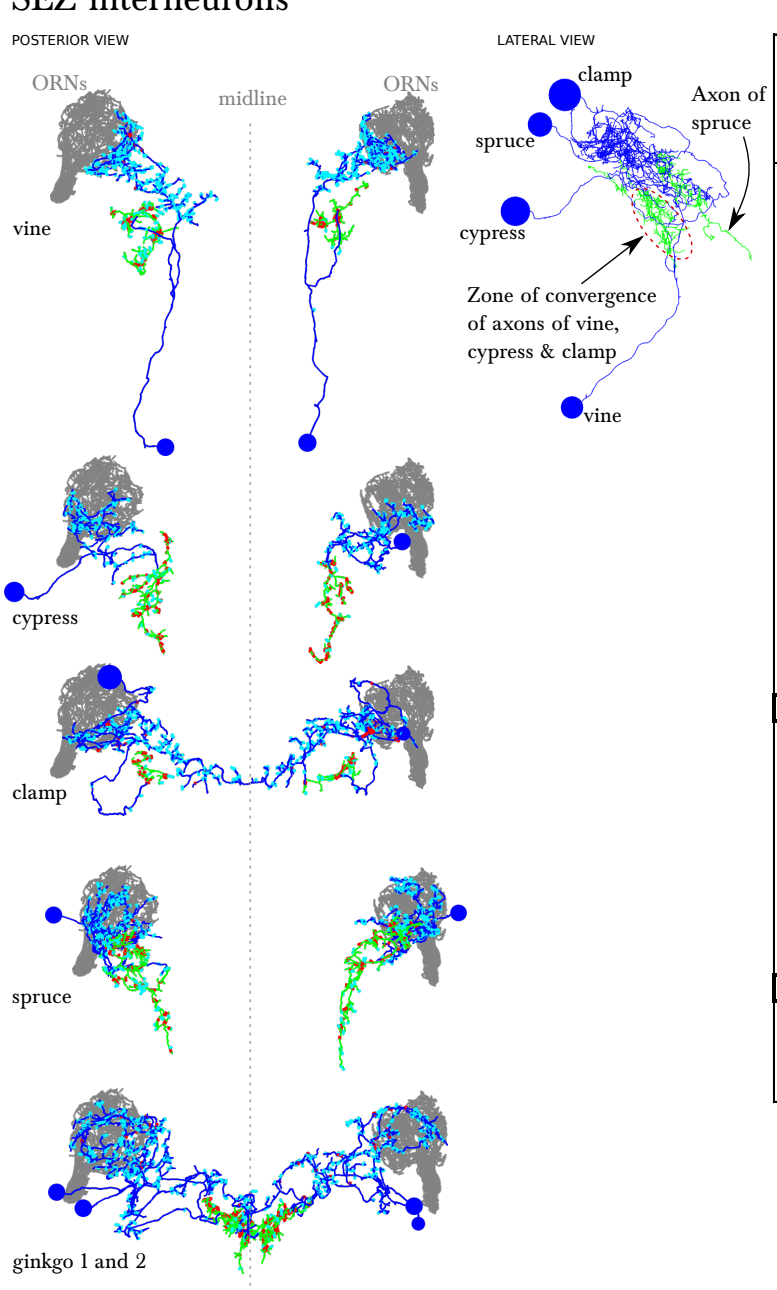

Right antennal lobe		SEZ interneurons: vine	cypress	clamp	spruce	ginkgo 1	ginkgo 2
ORNs + uPNs	1a	4					
	13a						
	22c						
	24a						
	30a		14		6		
	33a						
	35a	12		3			
	42a						
	42b	11					
	45a					9	6
	45b						
	47a/33b				8		4
	49a						
	59a						
	63a						
	67b		8		8		
	74a						
	82a						
	83a						
	85c						
	94a/94b				1		
%ORN Input		27	22	3	24	9	10
LNs	broad trio (3)	4	2		1		
	broad duet (2)	1					3
	keystone (2)		2				
	choosy LNs (2)	7	1	2		9	
	ventral LN			2			
	picky 0						
	picky 1						
	picky 2	2					10
	picky 3		12	2	12		4
	picky 4	2				9	4
%LN Input		17	16	5	14	18	20
Descending & modulatory	Descending						
	CSD (2)						
	IAL-1 (2)	2					
	tdc (2)		3				

Supplementary Figure 6: **Six SEZ neurons receive specific inputs from some ORNs and from some antennal lobe LNs.** *Left*, EM-reconstruction of the 6 SEZ neurons (vine, cypress, clamp, spruce and ginkgo 1 and 2), with their axons labeled green and their dendrites blue. Presynaptic sites in red and postsynaptic sites in cyan. *Middle*, 3 of these SEZ neurons project to the same unidentified region of the SEZ. Spruce projects to a more posterior area. Lateral view, anterior to the left. *Right*, table of percent of postsynaptic sites of a column neuron contributed by a row neuron, illustrating how some ORNs and LNs specifically target these SEZ neurons. We show only connections with at least two synapses, consistently found among homologous identified neurons in both the left and right antennal lobes. Percentages between 0 and 0.5 are removed. Notice how Picky LNs 2, 3 and 4 synapse strongly onto SEZ neurons.

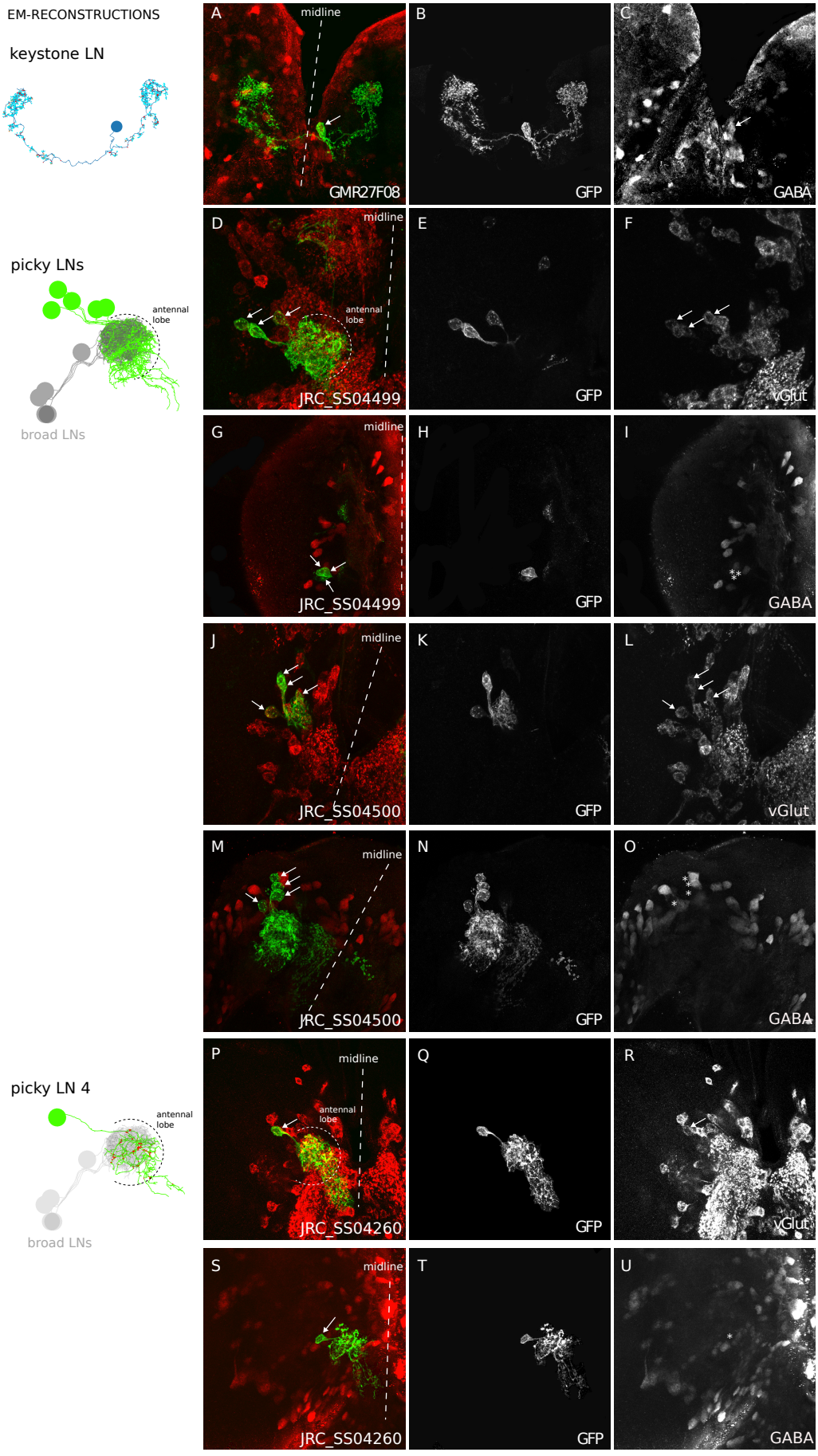

Supplementary Figure 7:
Neurotransmitters of keystone LN and Picky LNs. Genetic driver lines specific for keystone LN (GAL4 line GMR27F08) and Picky LNs (split-GAL4 lines JRC_SS04499, JRC_SS04500, JRC_SS04260) driving GFP expression specifically in these neurons were labeled with anti-GABA and anti-vGlut (**A-U**), and also anti-Chat (all negative; not shown). Keystone presents immunoreactivity to anti-GABA (textbfA-C), and at least 4 of the 5 Picky LNs are positive to anti-vGlut and negative to anti-GABA (**D-U**). These neurons derive from the BAla2 lineage (Das et al., 2013). JRC_SS04260 drives expression specifically and uniquely a Picky LN, likely Picky LN 4, which presents anti-vGLut immunoreactivity (**P-R**). *Left* unlettered panels show the homologous identified EM-reconstructed neurons, with Broad LNs in grey for reference. Asterisks mark the location of cell bodies when there is not labeling, such as in panels I, O and U. Broad LNs and Choosy LNs are GABAergic (see Thum et al., 2011 at fig. 2 D-G for Broad LNs and L-O for Choosy LNs).

a

Cluster 1: Alcohols	Cluster 2: Esters	Cluster 3: Pyrazines	Cluster 4: Aromatics 1	Cluster 5: Aromatics 2
1-butanol	Ethyl acetate	2-ethylpyrazine	Methyl salicylate	Benzaldehyde
1-hexanol	Propyl acetate	2-methoxypyrazine	2-methylphenol	Acetophenone
1-octen-3-ol	Pentyl acetate	2,3-diethylpyrazine	4-methylphenol	Anisole
1-heptanol	Isopentyl acetate	2-Isobutyl-3-methoxypyrazine		Methyleugenol
3-octanol	Ethyl butyrate	2,3-dimethylpyrazine		2,3-butanedione
1-nonanol	Geranyl acetate	2,5-dymethylpyrazine		cyclohexanone
E2-hexenal	Propanoic acid	Pyrazine		
2-heptanone	Carbon dioxide			

The color code is Alcohols, Esters, Pyrazines, Aromatics, Others

b

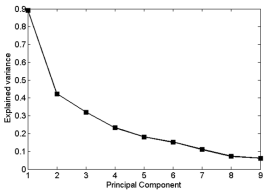

c

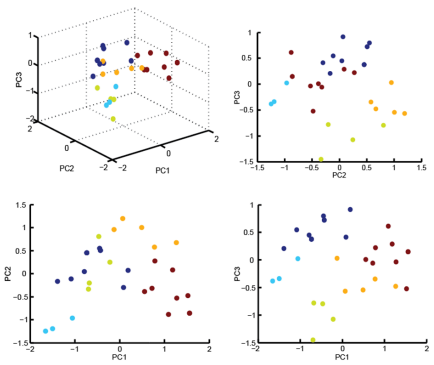

d

Cluster 1: Alcohols	Cluster 2: Esters	Cluster 3: Pyrazines	Cluster 4: Aromatics	Cluster 5: Mixed
1-butanol	Ethyl acetate	2-ethylpyrazine	Benzaldehyde	1-nonanol
1-hexanol	Propyl acetate	2-methoxypyrazine	Acetophenone	Pyrazine
1-octen-3-ol	Isopentyl acetate	2,3-dimethylpyrazine	Anisole	2,3-diethylpyrazine
1-heptanol	Ethyl butyrate	2,5-dymethylpyrazine		2-Isobutyl-3-methoxypyrazine
3-octanol	2,3-butanedione			Methyl salicylate
E2-hexenal				2-methylphenol
2-heptanone				4-methylphenol
cyclohexanone				Methyleugenol
Pentyl acetate				Geranyl acetate
				Propanoic acid
				Carbon dioxide

e

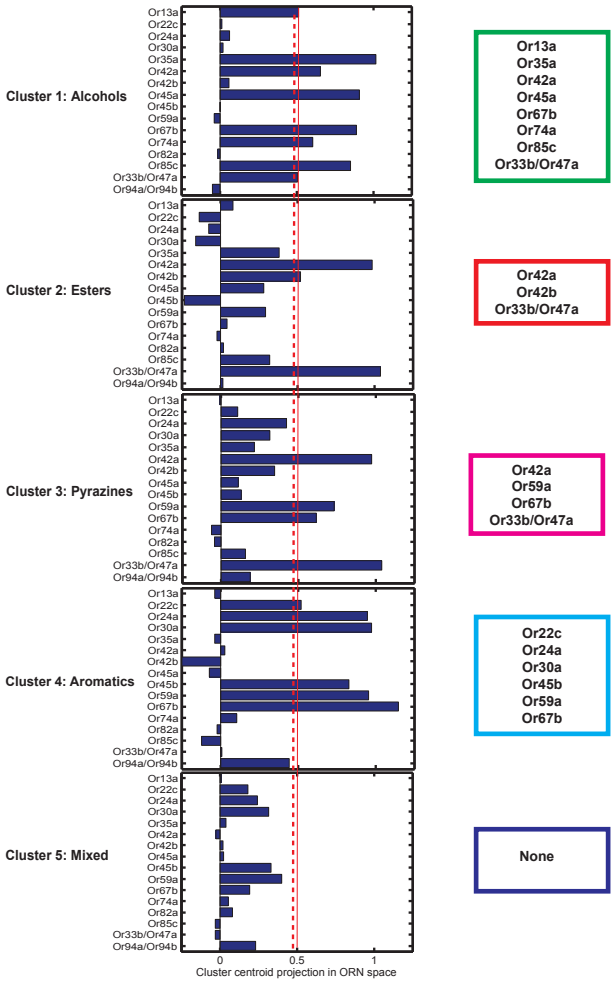

Supplementary Figure 8: **Principal component analysis of odors leading to a principled clustering of ORNs.** **a** Clustering of odors by odor-descriptor. Results of K-means clustering of odors in the 32 dimensional odor-descriptor space proposed in Haddad et al., 2008. Odors cluster into five groups that are well correlated with odor chemical type (alcohols, aromatics, esters, pyrazines, and others). **b-e** Clustering of odors by ORN response. **b** The variance explained for the odors in ORN response space as a function of the number of principal components (dimensions). The "elbow" of this curve is composed of the principal components used for the clustering analysis of the odors by ORN-response. **c** How the odors span the space of the first 3 principal components of ORN response space. The odors are individual points colored by which of the 5 clusters, calculated via an affinity propagation clustering algorithm, they belong to. **d** How each of the odors fit into the clusters in ORN response space. Each cluster tends to group odors of similar chemical type. **e** The ORNs that represent the centroid of each cluster, calculated using a threshold obtained via Otsu's method. See materials and methods for further details.

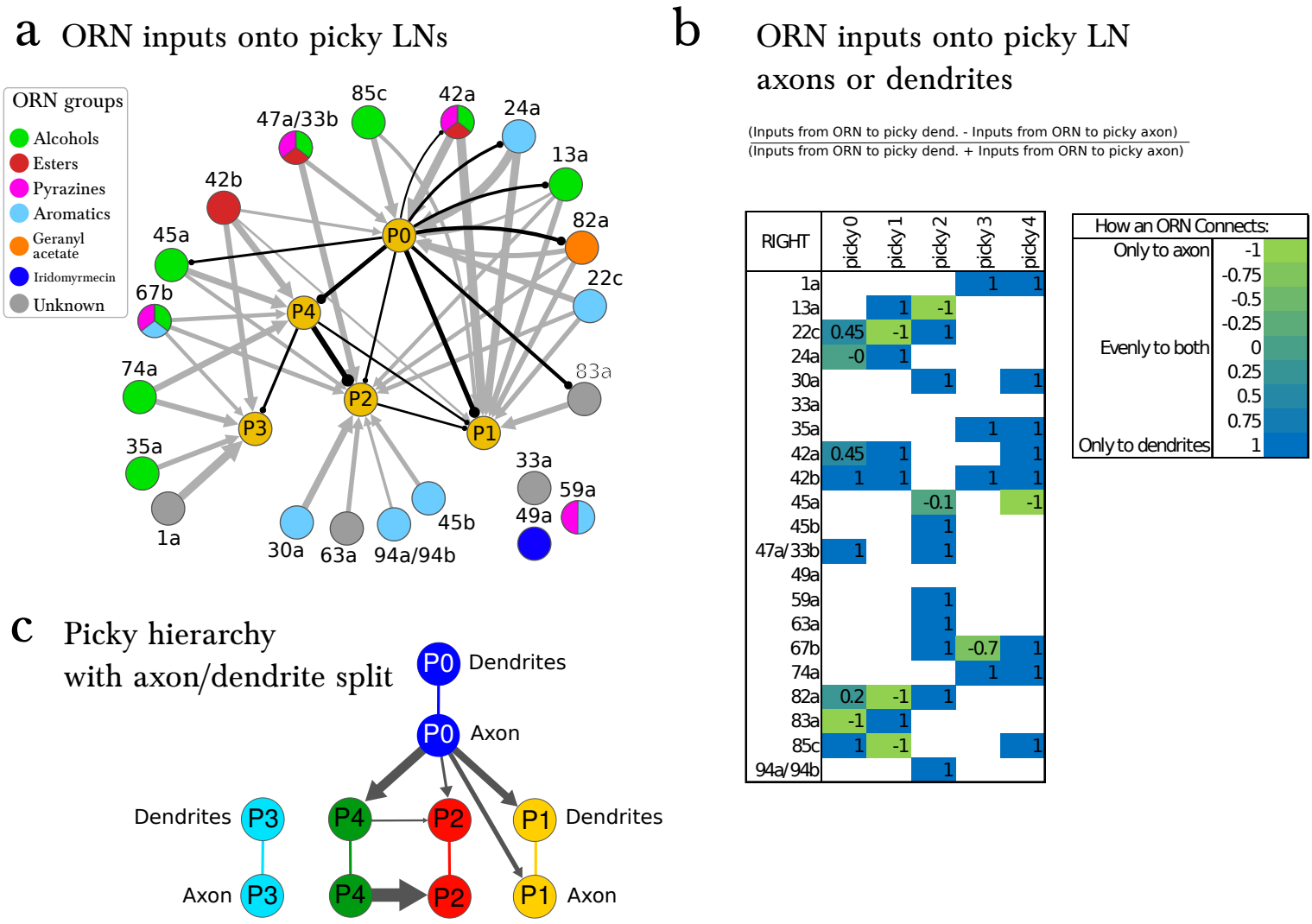

Supplementary Figure 9: **Pattern of ORN inputs onto Picky LNs.** **A** The connections of ORNs onto the hierarchy of Picky LNs. ORNs are colored by the groups emerging from the PCA analysis of odor tuning. Inhibitory connections from Picky LNs are shown in black (only connections with 2 or more synapses among bilaterally homologous neuron pairs are show). Excitatory connections from ORNs are shown in grey (only connections with 4 or more synapses among bilaterally homologous neuron pairs are shown). See adjacency matrix for the complete set of connections. The thickness of the arrows is proportional to the square root of the number of synapses. Some of these connections are axo-axonic (see *C*). **B** ORNs can synapse onto the Picky neurons at either their dendrites or their axons. This table shows values from -1 to 1 based on the written formula. Values between -1 and 0 correspond to the ORN synapsing more to the axon of the Picky LN than the dendrite, and values between 0 and 1 correspond to the ORN synapsing more to the dendrite of the Picky LN than the axon. Only consistent connections between ORNs and Picky dendrites or ORNs and Picky axons with a threshold of at least 2 consistent synapses per side are used to calculate these ratios. For values that are not 1 or -1, the value can differ from side to side. Because the threshold is lowered from that of *A*, more connections appear, but since we only consider connections consistent in how they connect to the Picky LNs (to dendrite or axon), some of the weakest connections also drop out compared to *A*. **C** The Picky LN hierarchy shown with the Picky LNs split into axon and dendrite, showing that not all connections are from the axon of a Picky LN to the dendrites of another. We are only showing connections that are consistent both in their motif (axo-axonic, dendro-dendritic, etc) and with a consistent threshold of 2 synapses on both sides. Because these criteria are more stringent than those used in *A*, some connections drop out (such as Picky LN 4 to Picky LN 3).